Enhancing Depression Mechanisms in Midbrain Dopamine Neurons Achieves Homeostatic Resilience

Allyson K. Friedman *et al.*

Science **344**, 313 (2014);
DOI: 10.1126/science.1249240

of transcription 3), a transcription factor that regulates DC differentiation (*9*), was identified as a lnc-DC–associated protein, and this was confirmed by independent immunoblot (Fig. 4A). RIP further verified the specificity of this interaction (Fig. 4B). Moreover, RNA FISH followed by immunofluorescence showed lnc-DC colocalized with STAT3 in the cytoplasm but not the nucleus of DCs (Fig. 4C), indicating that lnc-DC may regulate cytoplasmic STAT3 activity. Analysis of lnc-DC truncation mutants revealed that the 3′-end segment of lnc-DC (nucleotides 265 to 417) was sufficient to bind STAT3 (fig. S17A). RNA folding analyses (*26*) of this 3′ region indicated a stable stem-loop structure (fig. S17B), which might provide the necessary spatial conformation for the interaction. RIP (fig. S18A), biotin-RNA pull-down assay (fig. S18B), and confocal analysis (fig. S18C) with full-length or truncated STAT3 demonstrated that the C terminus of STAT3 (residues 583 to 770) interacted with lnc-DC. Because this portion contains Tyr^{705} (Y705), whose phosphorylation is crucial for STAT3 activation and nuclear translocation (*27*), we wondered whether the binding of lnc-DC affects STAT3 phosphorylation status. Immunoblotting revealed that STAT3 Y705 phosphorylation was reduced by lnc-DC knockdown in Mo-DC and mouse bone marrow cells (Fig. 4D and fig. S13D), and subsequent STAT3 nuclear translocation was decreased (fig. S19A). Ectopic expression of lnc-DC enhanced STAT3 luciferase reporter activity in human embryonic kidney 293 T cells (HEK293T cells) (fig. S19B) and STAT3 Y705 phosphorylation in THP1 cells (fig. S19C). Furthermore, our protein posttranslational modification analysis of STAT3 revealed that only Y705 phosphorylation was enhanced by lnc-DC (fig. S20 and table S1). These data suggest that cytoplasmic lnc-DC promotes STAT3 signaling.

The pharmacological inhibitor of STAT3, S3I-201, which targets the C-terminal structure of STAT3 (*28*), could attenuate lnc-DC interaction with STAT3 in a dose-dependent manner (Fig. 4E). Furthermore, transcriptome microarray analysis revealed that treatment of Mo-DC with S3I-201 resulted in similar effects on gene expression as seen with lnc-DC knockdown (Fig. 4F). Many known STAT3 target genes were affected by lnc-DC knockdown (fig. S21). Functionally, administration of STAT3 inhibitors impaired Mo-DC differentiation from monocytes and attenuated DC function in a manner similar to lnc-DC knockdown (fig. S22). Thus, we propose that lnc-DC promotes DC differentiation through STAT3 signaling.

Mass spectrometric analysis of STAT3-interacting proteins affected by lnc-DC led us to focus on SHP1 (fig. S23A), a protein tyrosine phosphatase and an important negative regulator of cellular signaling pathways, including Jak/STAT signaling. Coimmunoprecipitation confirmed that knockdown of lnc-DC promoted the association of SHP1 with STAT3 in Mo-DC (fig. S23, B and C), and overexpression of lnc-DC attenuated SHP1-STAT3 interaction in HEK293T cells (fig. S23, D and E). Furthermore, an in vitro phosphatase assay with recombinant human protein SHP1 showed that lnc-DC, but not the antisense control RNA, protected STAT3 from Y705 dephosphorylation by SHP1 (Fig. 4G). Taken together, our results demonstrate that, during DC differentiation, lnc-DC promotes STAT3 signaling by interacting with the C terminus of STAT3 to prevent dephosphorylation of STAT3 Y705 by SHP1 (fig. S24).

Our work suggests that lncRNAs can affect cellular differentiation and function by directly interacting with signaling molecules in the cytoplasm and regulating their posttranslational modification. Whether other cytoplasmic lncRNAs perform their functions in a manner similar to lnc-DC is currently unclear. lnc-DC, as a specific regulator of DC differentiation and function, may have potential relevance to clinical diseases involving DC dysfunction and may aid the design of DC vaccines with more potency to activate T cell responses.

References and Notes

1. P. Johnsson, L. Lipovich, D. Grandér, K. V. Morris, *Biochim. Biophys. Acta* **1840**, 1063–1071 (2014).
2. O. Wapinski, H. Y. Chang, *Trends Cell Biol.* **21**, 354–361 (2011).
3. M. Sauvageau *et al.*, *eLife* **2**, e01749 (2013).
4. J. L. Rinn, H. Y. Chang, *Annu. Rev. Biochem.* **81**, 145–166 (2012).
5. Z. Li *et al.*, *Proc. Natl. Acad. Sci. U.S.A.* **111**, 1002–1007 (2014).
6. S. Carpenter *et al.*, *Science* **341**, 789–792 (2013).
7. G. Hu *et al.*, *Nat. Immunol.* **14**, 1190–1198 (2013).
8. P. Guermonprez *et al.*, *Nat. Med.* **19**, 730–738 (2013).
9. Y. Laouar, T. Welte, X. Y. Fu, R. A. Flavell, *Immunity* **19**, 903–912 (2003).
10. S. Carotta *et al.*, *Immunity* **32**, 628–641 (2010).
11. M. Merad, P. Sathe, J. Helft, J. Miller, A. Mortha, *Annu. Rev. Immunol.* **31**, 563–604 (2013).
12. L. A. O'Neill, F. J. Sheedy, C. E. McCoy, *Nat. Rev. Immunol.* **11**, 163–175 (2011).
13. M. S. Ebert, P. A. Sharp, *Cell* **149**, 515–524 (2012).
14. T. R. Mercer, J. S. Mattick, *Nat. Struct. Mol. Biol.* **20**, 300–307 (2013).
15. K. V. Morris, S. Santoso, A. M. Turner, C. Pastori, P. G. Hawkins, *PLOS Genet.* **4**, e1000258 (2008).
16. P. Johnsson *et al.*, *Nat. Struct. Mol. Biol.* **20**, 440–446 (2013).
17. M. Huarte *et al.*, *Cell* **142**, 409–419 (2010).
18. U. A. Ørom *et al.*, *Cell* **143**, 46–58 (2010).
19. M. Cesana *et al.*, *Cell* **147**, 358–369 (2011).
20. Y. Tay *et al.*, *Cell* **147**, 344–357 (2011).
21. C. Gong, L. E. Maquat, *Nature* **470**, 284–288 (2011).
22. See supplementary materials and methods on *Science* Online.
23. M. Haniffa *et al.*, *Immunity* **37**, 60–73 (2012).
24. S. Djebali *et al.*, *Nature* **489**, 101–108 (2012).
25. A. Guerriero, P. B. Langmuir, L. M. Spain, E. W. Scott, *Blood* **95**, 879–885 (2000).
26. A. R. Gruber, R. Lorenz, S. H. Bernhart, R. Neuböck, I. L. Hofacker, *Nucleic Acids Res.* **36** (suppl. 2), W70–W74 (2008).
27. J. J. O'Shea, R. Plenge, *Immunity* **36**, 542–550 (2012).
28. K. Siddiquee *et al.*, *Proc. Natl. Acad. Sci. U.S.A.* **104**, 7391–7396 (2007).

Acknowledgments: We thank M. Jin and P. Ma for technical assistance; W. Ge, P. Zhang, and X. Xu for helpful discussions; and Q. Li of Genminix Informatics for bioinformatics assistance. The data presented in this paper are tabulated in the main paper and in the supplementary materials. Our transcriptome microarray data and RNA-seq data are deposited in Gene Expression Omnibus (GEO) under the accession nos. GSE54143 and GSE54401, respectively, and our ChIP-seq data are deposited in GEO under the accession no. GSE43036. This work is supported by grants from the National Key Basic Research Program of China (2013CB530502) and the National Natural Science Foundation of China (31390431, 81230074, and 81123006). X.C. and P.W. designed the experiments; P.W., Y.X., Y.H., L.L., C.W., S.X., Z.J., J.X., and Q.L. performed the experiments; X.C. and P.W. analyzed data and wrote the paper; and X.C. was responsible for research supervision, coordination, and strategy. We declare no competing financial interests.

Supplementary Materials

www.sciencemag.org/content/344/6181/310/suppl/DC1
Materials and Methods
Figs. S1 to S24
Tables S1
References (*29*–*38*)

28 January 2014; accepted 26 March 2014
10.1126/science.1251456

Enhancing Depression Mechanisms in Midbrain Dopamine Neurons Achieves Homeostatic Resilience

Allyson K. Friedman,[1] Jessica J. Walsh,[1,2] Barbara Juarez,[1,2] Stacy M. Ku,[1,2] Dipesh Chaudhury,[1] Jing Wang,[3] Xianting Li,[3] David M. Dietz,[4] Nina Pan,[3] Vincent F. Vialou,[4] Rachael L. Neve,[5] Zhenyu Yue,[3,4] Ming-Hu Han[1,4]*

Typical therapies try to reverse pathogenic mechanisms. Here, we describe treatment effects achieved by enhancing depression-causing mechanisms in ventral tegmental area (VTA) dopamine (DA) neurons. In a social defeat stress model of depression, depressed (susceptible) mice display hyperactivity of VTA DA neurons, caused by an up-regulated hyperpolarization-activated current (I_h). Mice resilient to social defeat stress, however, exhibit stable normal firing of these neurons. Unexpectedly, resilient mice had an even larger I_h, which was observed in parallel with increased potassium (K^+) channel currents. Experimentally further enhancing I_h or optogenetically increasing the hyperactivity of VTA DA neurons in susceptible mice completely reversed depression-related behaviors, an antidepressant effect achieved through resilience-like, projection-specific homeostatic plasticity. These results indicate a potential therapeutic path of promoting natural resilience for depression treatment.

Resilience is the brain's capacity to cope with environmental stress and to achieve stable psychological functioning in response to prolonged stress (*1*–*3*). Multiple psychological techniques are used to promote resilience to stress. Specifically, active coping strategies, in

which qualities or perceptions of stressors are reassessed, as opposed to avoidant coping, have proven to promote behavioral adaptability and achieve psychological resilience (*4*, *5*). To understand the neurobiological mechanisms underlying stress resilience, tremendous efforts have been made to investigate the genetic, molecular, and developmental aspects of this phenomenon (*1*, *3*, *6*, *7*). Despite many advances, the neurophysiological processes determining the brain's ability to cope with stress are still poorly understood.

Multiple lines of evidence implicate dysregulation in the brain's reward neural circuit in depression (*1*, *8*–*11*). In a well-established chronic social defeat model of depression, susceptible and resilient phenotypes have been successfully segregated after a 10-day social defeat paradigm (*1*, *9*, *12*, *13*). Multiple depressive symptoms in susceptible mice have been causally linked to hyperactivity of ventral tegmental area (VTA) dopamine (DA) neurons (*1*, *9*, *12*). Optogenetic activation of these neurons promotes susceptible phenotype, whereas optogenetic reduction of the hyperactivity reverses depression-related behaviors (*9*). This increase in VTA DA neuron firing in susceptible mice is known to be intrinsically induced by up-regulation of hyperpolarization-activated cation channel–mediated current (I_h), an excitatory driving force in VTA DA neurons (*12*, *14*, *15*). Pharmacological reduction of the increased I_h in susceptible mice reverses depression-related symptoms (*12*). Chronic antidepressant fluoxetine treatment normalizes the hyperactivity and decreases I_h in these neurons (*12*). These observations suggest that hyperactivity and increased excitatory I_h in VTA DA neurons are both pathophysiological adaptations underlying the susceptible phenotype.

To understand the neurophysiological mechanisms of the resilient phenotype after chronic social stress, we used tyrosine hydroxylase–driven green fluorescent protein (TH-GFP) transgenic mice to visualize and reliably record from VTA DA neurons (fig. S1A). TH-GFP mice that undergo chronic social defeat stress reliably separate into either susceptible or resilient phenotypes on the basis of social interaction ratios (fig. S1, B and C) (*1*, *9*, *12*, *13*). Susceptible TH-GFP mice showed social avoidance, spending significantly less time in the interaction zone, whereas resilient mice spent a significant amount of time with the social target, similar to the time spent by control mice (fig. S1, D to G). Susceptible mice also display other depression-related anhedonic behaviors (fig. S1H) (*1*, *7*). We confirmed pathophysiological hyperactivity in the GFP-visualized DA neurons of susceptible TH-GFP mice (fig. S1I), whereas the pacemaker firing pattern was the same in the three groups. Overall, the resilient TH-GFP mice exhibited a stable control level firing of VTA DA neurons and appeared not to have undergone any pathogenic changes at cellular and behavioral levels in response to chronic social defeat stress (fig. S1, D to I, and fig. S2).

We next investigated whether the pathophysiological increase in I_h current is normalized in resilient mice. We performed whole-cell voltage-clamp recordings in GFP^+ VTA DA neurons in brain slices from control, susceptible, and resilient TH-GFP mice. In accordance with previous findings (*12*), I_h was increased in susceptible mice (Fig. 1A). However, unexpectedly, rather than a normalization of the I_h levels in resilient mice, the resilient phenotype showed an even larger significant increase in I_h when compared with susceptible and control mice (Fig. 1A). This was surprising and unanticipated because an increase in I_h was viewed as a stress-induced, pathological ion mechanism in susceptible mice.

To understand how VTA DA neurons in resilient mice maintain a level of firing similar to that of control mice with this extremely larger I_h, we focused on K^+ channels, an inhibitory driving force that was up-regulated selectively in the resilient subgroup in a previous microarray analysis (*1*). The VTA DA neurons of resilient mice, which displayed a further enhanced I_h, simultaneously exhibited significantly increased K^+ channel–mediated peak and sustained currents (Fig. 1B), which implicate multiple K^+ channel types mediating this increase in K^+ currents.

To investigate a possible benefit of resilient mice recruiting these extra channel functions, we measured intrinsic excitabilities of VTA DA neurons in the three groups. In response to a series of current injections, we observed an increase in spike number in susceptible mice and, inversely, a reduction in spike number in resilient mice, as compared with control mice (Fig. 1C). This suggests that the reestablished status of VTA DA neurons in resilient mice is more stable and less vulnerable to perturbations than that of controls.

The up-regulation of I_h in VTA DA neurons of resilient mice may be driving the neuronal firing extremely high and triggering a self-tuning K^+ current mechanism to bring the extreme firing back to control (fig. S3). This in turn normalizes the depressive behaviors. To determine whether enhancing I_h current in susceptible mice can trigger this hypothesized homeostatic plasticity observed in the resilient mice, we pharmacologically increased I_h through in vivo infusion of an I_h potentiator, lamotrigine, into the VTA of TH-GFP susceptible mice. Lamotrigine is known to enhance I_h (*16*) and is clinically used as a mood stabilizer to treat the depressed phase of bipolar disorder with uncertain mechanisms (*17*). In brain slices, bath application of lamotrigine increased I_h and the firing rate of VTA DA neurons (fig. S4). Consistently, a single in vivo infusion into the VTA of susceptible mice increased social avoidance (fig. S5). To determine whether repeated enhancement of this current can induce a homeostatic compensatory response, we performed repeated 5-day local infusions of lamotrigine (0.1 μg) into the VTA of susceptible TH-GFP mice (Fig. 1, D and E, and fig. S6A), because it is known that 4 to 5 days is sufficient to induce stable changes in social behaviors (*18*). After 5 days of local infusion, we observed a profound reversal of social avoidance, with more time spent interacting with a social target (Fig. 1F) and reduced time in the corner zone (fig. S6B), without adverse effects on locomotion (fig. S6C). The defeat-induced deficit in sucrose preference was also significantly reversed after repeated lamotrigine infusion (Fig. 1G), which indicated an overall resilient, antidepressant effect, without affecting the behaviors in either control or resilient mice (fig. S7 and S8).

Consistent with the behavioral antidepressant effect, the hyperactivity of VTA DA neurons in susceptible mice was normalized after I_h potentiation via lamotrigine (Fig. 1H). To examine the ionic mechanisms that underlie this promotion of resilience, we determined the effects of repeated lamotrigine infusion on I_h and K^+ currents. We observed a marked increase in I_h (Fig. 1I) and a compensatory increase in K^+ currents (Fig. 1J), a phenomenon not observed at lower doses (fig. S9). Consistently, these ionic changes induced a reduction in DA neuron excitability in the lamotrigine-treated animals (Fig. 1K), as compared with vehicle-treated controls. These data describe a possible mechanism of lamotrigine's mood-stabilizing efficacy.

Although one of the actions of lamotrigine is known to increase I_h current, lamotrigine has other effects on neurons, such as blockade of sodium channels (*19*). To specifically assess the role enhanced I_h has in VTA DA neurons, we selectively overexpressed hyperpolarization-activated and cyclic nucleotide–gated channel 2 (HCN2), a channel isoform that mediates I_h current (*20*). We used a combination of TH-Cre mice and Cre-inducible loxP-STOP-loxP herpes simplex virus with enhanced yellow fluorescent protein (HSV-LS1L-HCN2-eYFP) and HSV-LS1L-eYFP as control. The HSV vectors allow for the rapid expression of HCN2 over 5 days (*18*). The Cre-inducible vectors were injected bilaterally into the VTA of TH-Cre transgenic mice to ensure specific expression in DA neurons (Fig. 2, A and B). Functional validation 24 hours after injection successfully showed an increase in I_h (Fig. 2C) and corresponding increase in firing (Fig. 2D). Next, we injected HSV-LS1L-HCN2-eYFP or HSV-LS1L-eYFP into the VTA of susceptible TH-Cre mice and carried out the behavioral and electrophysiological measurements 4 to 6 days after viral injection (Fig. 2, E and F). Overexpression of HCN2 in the VTA DA neurons of susceptible mice resulted in a reversal of social avoidance (Fig. 2G and fig. S10A) and other depressive behaviors (Fig. 2, H and I), with no affect on locomotion (fig. S10B).

[1]Department of Pharmacology and Systems Therapeutics, Icahn School of Medicine at Mount Sinai, New York, NY 10029, USA. [2]Neuroscience Program, Graduate School of Biomedical Sciences, Icahn School of Medicine at Mount Sinai, New York, NY 10029, USA. [3]Department of Neurology, Icahn School of Medicine at Mount Sinai, New York, NY 10029, USA. [4]Department of Neuroscience and Friedman Brain Institute, Icahn School of Medicine at Mount Sinai, New York, NY 10029, USA. [5]McGovern Institute for Brain Research, Massachusetts Institute of Technology, Cambridge, MA 02139, USA.

*Corresponding author. E-mail: ming-hu.han@mssm.edu

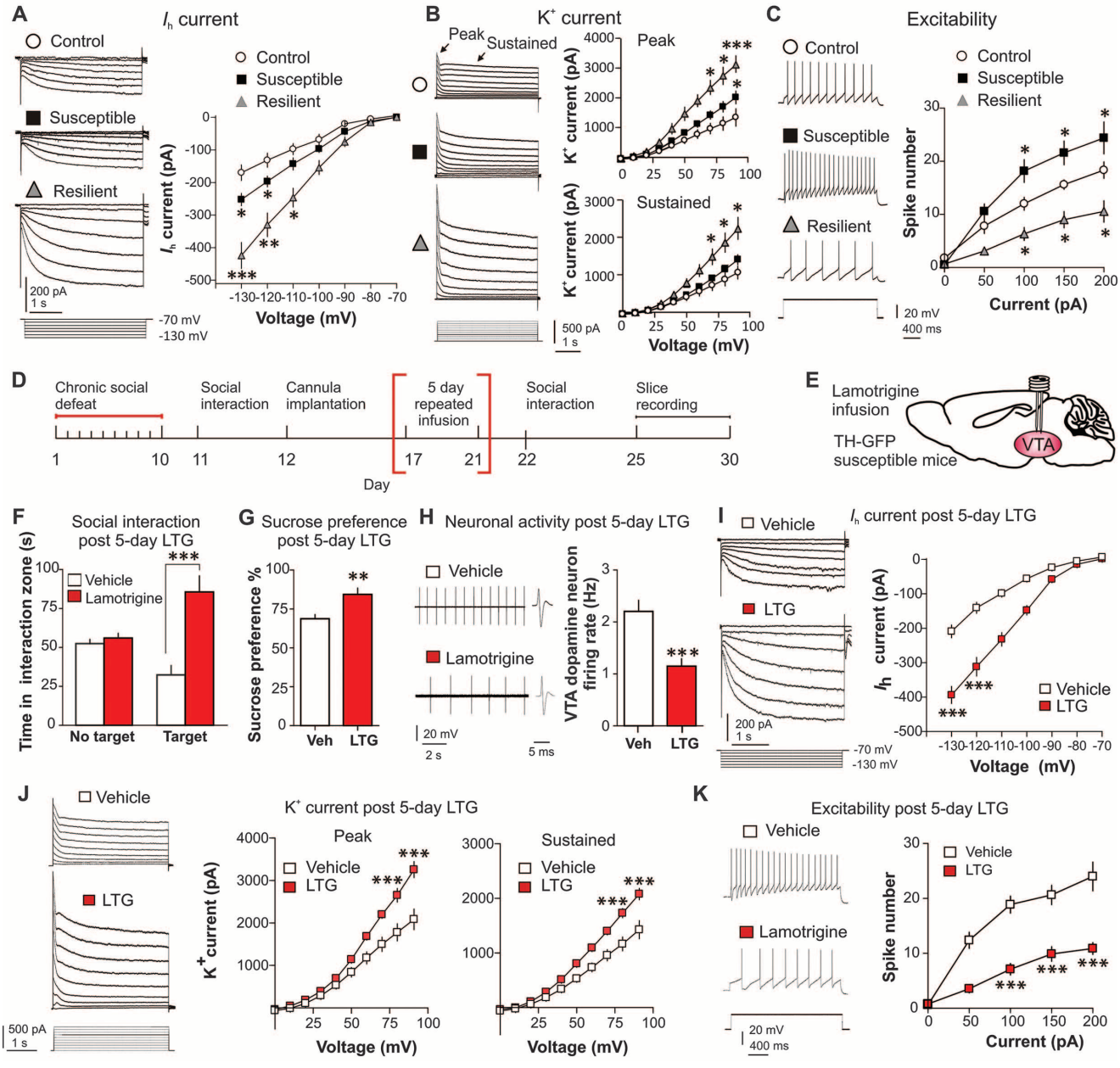

Fig. 1. The resilient phenotype shows dramatically increased I_h and K^+ channel currents in VTA DA neurons, and repeated infusion of I_h potentiator lamotrigine to the VTA of susceptible mice achieves antidepressant effects by inducing resilience-like homeostatic plasticity. (**A**) I_h sample traces and statistical data for control (open circles), susceptible (filled black squares), and resilient (filled gray triangles) mice. At −130 mV, $F_{(2,47)} = 19.19$, $P < 0.0001$; at −120 mV, $F_{(2,62)} = 17.69$, $P < 0.001$; $n = 12$ to 22 cells from 8 to 10 mice per group. Post hoc analysis at −130 mV shows a significant increase in I_h in susceptible mice ($t_{32} = 2.65$, $P < 0.05$) and an even significantly larger I_h increase in the resilient subgroup ($t_{24} = 5.24$, $P < 0.001$) compared with the control. (**B**) Sample traces and statistical data of isolated K^+ channel–mediated currents recorded from VTA DA neurons show that resilient mice have significantly increased peak and sustained phases of K^+ currents. At +90 mV, $F_{(2,58)} = 15.129$, $P < 0.001$; $n =$ 14 to 23 cells from 9 to 10 mice per group. Post hoc analysis shows a slight increase in peak K^+ currents in susceptible mice ($t_{41} = 2.62$, $P < 0.05$) and a larger increase in the resilient subgroup ($t_{36} = 5.25$, $P < 0.001$) compared with the control. (**C**) Susceptible mice display increased DA neuron excitability, whereas resilient mice display a reduction, after incremental steps in current injections (50, 100, 150, and 200 pA) compared with controls [at 100 pA: $F_{(2,28)} = 12.00$, $P <$ 0.001; at 150 pA $F_{(2,28)} = 12.66$, $P < 0.001$; and at 200 pA $F_{(2,25)} = 8.86$, $P <$ 0.001]. Post hoc analysis of susceptible and resilient compared with control mice for 100 and 150 and 200 pA currents at $P < 0.05$ ($n = 8$ to 12 cells from 7 to 8 mice per group). (**D** and **E**) Experimental timeline and schematic. (**F**) Five days of 4-min daily bilateral infusions of lamotrigine (LTG, 0.1 μg) or vehicle into the VTA reversed social avoidance ($t_{18} = 5.79$, $P < 0.001$; $n = 10$) and (**G**) sucrose preference ($t_{18} = 3.25$, $P < 0.01$; $n = 10$). (**H**) Sample traces and statistical data of VTA DA neuron firing in susceptible mice after repeated infusion of vehicle compared with lamotrigine infusions ($t_{32} = 4.10$, $P < 0.001$; $n = 17$ cells from 7 to 9 mice per group). (**I**) Sample traces and statistical data of I_h in susceptible mice after repeated infusion of vehicle (open squares) or lamotrigine (filled red squares) (at −130 mV: $t_{13} = 6.99$, $P < 0.0001$; at −120 mV: $t_{13} = 5.88$, $P < 0.0001$; $n = 7$ to 8 cells from 6 to 8 mice per group). (**J**) Sample traces and statistical data of K^+ currents in susceptible mice after repeated infusion of vehicle or lamotrigine: peak (at +20 mV: $t_{19} = 5.03$, $P < 0.001$; at +10 mV: $t_{19} = 5.92$, $P < 0.001$) and sustained (at +20 mV: $t_{19} = 5.95$, $P < 0.001$; at +10 mV: $t_{19} = 6.81$, $P < 0.001$; $n = 10$ to 11 cells from 7 to 9 mice per group). (**K**) Sample traces obtained at 100 pA current injection and statistical data of decreased excitability in susceptible mice infused with lamotrigine compared with vehicle (at 100 pA: $t_{15} = 6.41$, $P < 0.0001$; at 150 pA: $t_{15} = 4.93$, $P < 0.001$; at 200 pA: $t_{15} = 4.56$, $P < 0.001$; $n = 8$ to 9 cells from 7 to 9 mice per group). Error bars, ±SEM. *$P < 0.05$, **$P < 0.01$, ***$P < 0.001$.

After DA neuron–specific expression of HCN2 in susceptible mice, a robust reduction in hyperactivity was found in HCN2-expressing DA neurons, as compared with eYFP control neurons (Fig. 2J). We observed a significant increase in I_h current in HCN2-expressing cells (Fig. 2K), and in conjunction, we observed a significant increase in the K^+ currents (Fig. 2L), resulting in an overall reduction in excitability of these neurons (Fig. 2M).

Whereas excessively potentiating I_h resulted in a homeostatic up-regulation of K^+ channel function in VTA DA neurons of susceptible mice, this K^+ current compensation may be caused directly by the hyperactivity induced by I_h potentiation. In primary neuronal cultures, excessive hyperactivity can induce homeostatic up-regulation of K^+ channel–mediated current (*21*). We thus asked whether direct excessive activation of VTA DA neurons in susceptible mice could induce a functional K^+ channel counteraction that would normalize

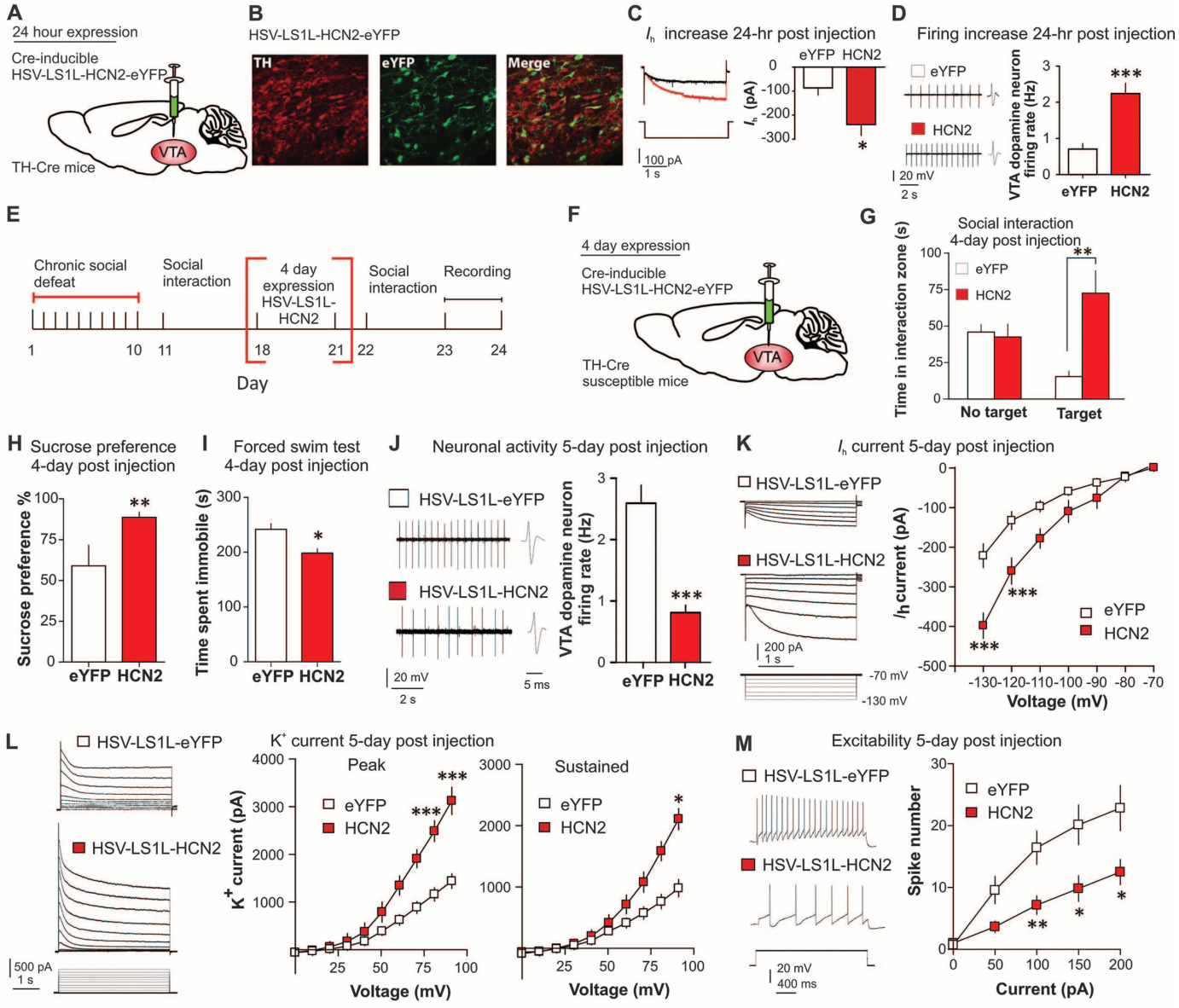

Fig. 2. DA neuron–specific overexpression of HCN2 channel induces an antidepressant behavioral effect and triggers a homeostatic response via an increase in compensatory K^+ currents. (**A**) Cre-inducible HSV-LS1L-HCN2-eYFP injection into the VTA of TH-Cre mice. (**B**) Confocal image showing colocalization (merge) of Cre-induced HCN2 (eYFP) expression in VTA DA neurons (TH) of TH-Cre mice. Quantification shows that HCN2-expressing TH^+ cells were 47 ± 4% of total TH^+ neurons in the VTA, and there was no expression of HCN2 in TH^- neurons (2 to 3 sections per mouse; $n = 4$). Scale bar, 100 μm; green, eYFP; red, TH. (**C**) Virally expressed HCN2 significantly increases I_h ($t_{13} = 2.73$, $P < 0.05$; $n = 7$ to 8 cells from each group, 3 mice per group) and (**D**) firing rate ($t_{25} = 6.86$, $P < 0.0001$; $n = 13$ to 14 cells from 4 mice per group) in VTA DA neurons as compared with control (eYFP) 24 hours after injection. (**E** and **F**) Experimental timeline and schematic. Behavioral effects of susceptible mice expressing HSV-LS1L-HCN2-eYFP or control HSV-LS1L-eYFP in DA neurons of the VTA on (**G**) social interaction test ($t_{22} = 3.72$, $P < 0.01$; $n = 12$); (**H**) sucrose preference test ($t_{18} = 3.40$, $P < 0.01$; $n = 10$); and (**I**) immobility time during forced swim test ($t_{18} = 2.87$, $P < 0.05$; $n = 10$). (**J** to **L**) Neuronal effects of 6 days of expression of HSV-LS1L-HCN2-eYFP (filled red squares) compared with HSV-LS1L-eYFP (open squares) in DA neurons of the VTA in susceptible mice on (J) firing rate ($t_{19} = 5.48$, $P < 0.0001$; $n = 10$ to 11); (K) I_h measurements (at –130 mV: $t_{22} = 4.51$, $P < 0.001$; at –120 mV: $t_{18} = 3.25$, $P < 0.005$); and (L) K^+ currents (–70 mV to +20 mV/10 mV step): peak (at +20 mV: $t_{16} = 5.70$, $P < 0.001$; at +10 mV: $t_{16} = 5.28$, $P < 0.001$); sustained (at +20 mV: $t_{16} = 2.480$, $P < 0.05$). (**M**) Sample traces at 100 pA current injection and statistical data of decreased excitability in susceptible mice expressing HCN2 compared with eYFP control (at 100 pA: $t_{12} = 3.21$, $P < 0.01$; at 150 pA: $t_{12} = 2.73$, $P < 0.05$; at 200 pA: $t_{12} = 2.54$, $P < 0.05$; $n = 7$ cells from 6 to 7 mice per group). Error bars, ±SEM. *$P < 0.05$, **$P < 0.01$, ***$P < 0.001$.

the hyperactivity of these neurons and depression-related behaviors. We examined social interaction behaviors and the channel functions after repeated optogenetic activation of VTA DA neurons in susceptible mice—further increasing the hyperactivity in susceptible mice. We injected Cre-inducible adenovirus-associated channelrhodopsin-2 (AAV-DIO-ChR2-eYFP) or control vector (AAV-DIO-eYFP) into the VTA of susceptible TH-Cre mice to selectively express ChR2 in VTA DA neurons (Fig. 3, A to C) (*9*, *22*, *23*). Bilateral implantable optic fibers were placed above the VTA (fig. S11A) for blue light photostimulation (five pulses, 20 Hz/10-s period) (Fig. 3, D and E) of DA neurons in susceptible mice, mimicking a validated in vivo firing pattern (*9*, *12*, *23*, *24*). After 5 days of 20-min photostimulation, susceptible mice with viral expression of ChR2 showed reduced social avoidance (Fig. 3F and fig. S11B) and reduced depressive behaviors (Fig. 3, G and H), without adverse effects on locomotion (fig. S11C). Excessive optogenetic activation of VTA DA neurons in susceptible mice reduced firing rate (Fig. 3I) and increased K^+ currents (Fig. 3J) in the ChR2-infected neurons, without altering I_h (fig. S11D). Consistent with the ionic alterations, we found a reduction in excitability of the ChR2-infected neurons (Fig. 3K).

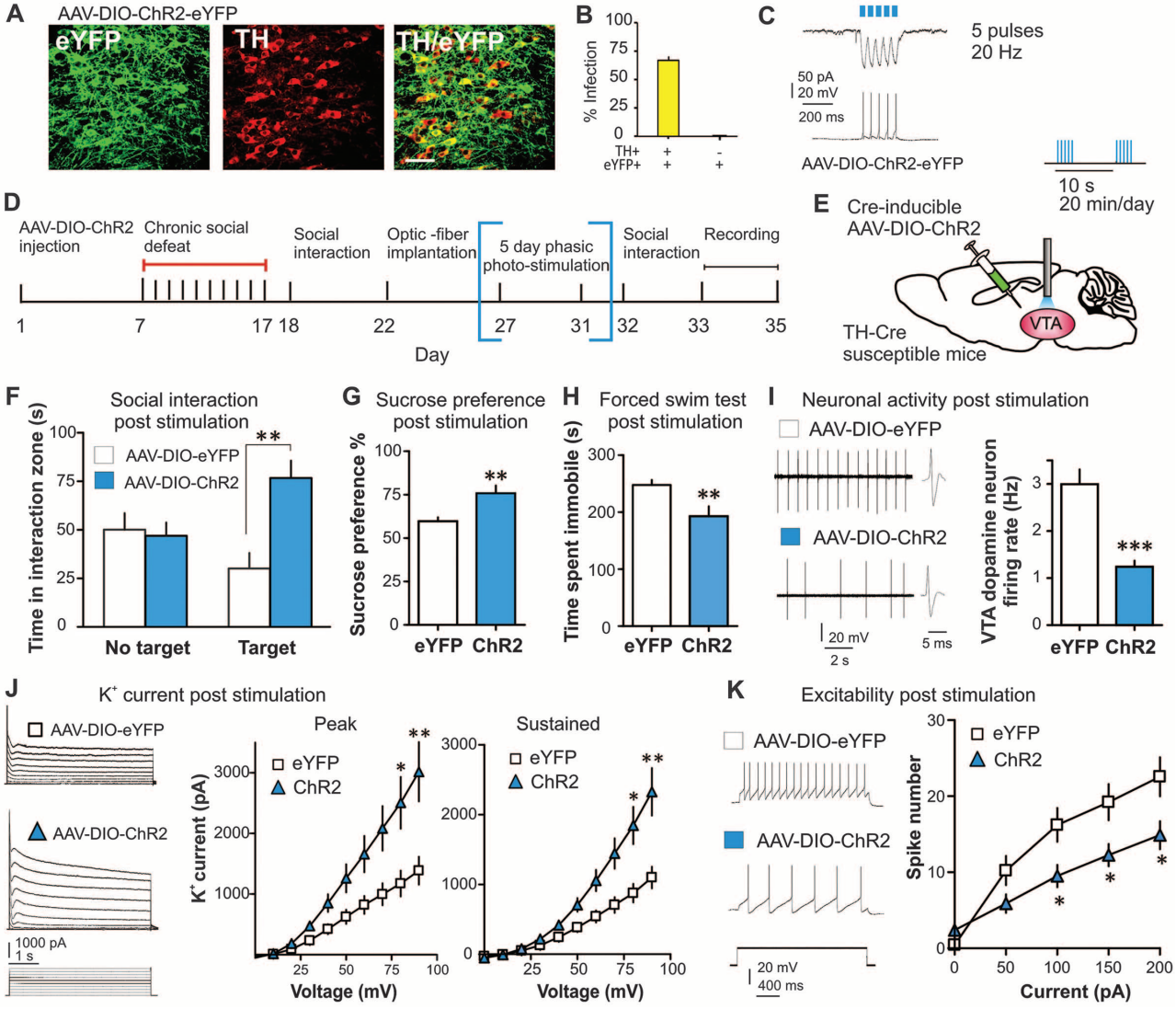

Fig. 3. Repeated optogenetic stimulation of VTA DA neurons normalizes the depressed phenotype and induces a significant compensation in K^+ currents. (**A**) Cell type–specific AAV-DIO-ChR2-eYFP expression (green) in VTA DA neurons (red) of TH-Cre mice. Scale bar, 100 μm. (**B**) Quantification shows that ChR2-expressing TH^+ cells are 67 ± 4% of total TH^+ neurons in the VTA, and there was no expression of ChR2 in TH^- neurons (n = 2 to 3 sections per mouse; n = 5 animals). (**C**) Voltage-clamp (upper trace) and current-clamp (lower trace) recordings from DA neurons in VTA slices. Five short bursts (20 Hz, 40 ms) of blue light (470 nm) induce temporally precise inward photocurrents and corresponding action potentials. (**D**) Experimental timeline. (**E**) Localization of bilateral viral injection and optic-fiber implantation used for in vivo delivery of blue light in susceptible TH-Cre mice. Phasic light pulses (470 nm, 20 Hz, five pulses/10 s) were delivered 20 min a day for five consecutive days. (**F**) After 5 days (20 min/day) of phasic stimulation of DA neurons, susceptible animals expressing ChR2 have increased social interaction (t_{22} = 3.59, P < 0.01; n = 12); (**G**) increased sucrose preference (t_{20} = 3.25, P < 0.01; n = 11); and (**H**) decreased immobility time during forced swim test (t_{18} = 2.89, P < 0.01; n = 10). (**I**) Sample traces and statistical data of VTA DA neuron firing in susceptible mice after chronic excessive activation (t_{23} = 6.25, P < 0.001; 12 to 13 cells from 6 mice per group). (**J**) Sample traces and statistical data of K^+ currents recorded from VTA DA neurons in brain slices from eYFP and ChR2-expressing neurons. Excessive optical activation of VTA DA neurons significantly increased the peak (at +20 mV: t_{19} = 3.08, P < 0.01; at +10 mV: t_{19} = 2.83, P < 0.05; at 0 mV) and sustained (at +20 mV: t_{19} = 3.53, P < 0.01; +10 mV: t_{19} = 3.18, P < 0.05) phases of K^+ currents. (**K**) Sample traces at 100 pA current injection and statistical data of decreased excitability in susceptible mice expressing ChR2 compared with eYFP (at 100 pA: t_{15} = 2.47, P < 0.05; at 150 pA: t_{15} = 2.41, P < 0.05; at 200 pA: t_{15} = 2.32, P < 0.05; n = 8 to 9 cells from 6 to 8 mice per group). Error bars, ±SEM. *P < 0.05, **P < 0.01, ***P < 0.001.

Recent studies show that VTA DA neurons are heterogeneous (*9*, *11*, *25*, *26*). For instance, VTA DA neurons projecting to nucleus accumbens (NAc) exhibit a large I_h, whereas medial prefrontal cortex (mPFC)–projecting VTA DA neurons have a small I_h (*26*). Utilizing retrograde tracers, we found that I_h alterations in response to chronic social defeat occur specifically in NAc-projecting VTA neurons but not in mPFC-projecting VTA neurons (Fig. 4, A and H, and figs. S12A and S13A). Note that the homeostatic plasticity that occurs in response to projection-specific HCN2 overexpression and repeated optogenetic stimulation is unique to the VTA-NAc projection (Fig. 4, B to G, and fig. S12). A different form of plasticity occurred in VTA-mPFC neurons: To our surprise, HCN2 overexpression had no effects on behavior, firing, I_h, and K^+ currents (Fig. 4, I to K, and fig. S13, B to G), whereas repeated optogenetic stimulation reversed social avoidance accompanied by a firing increase and a K^+ current decrease, the physiological changes opposite to those seen in VTA-NAc neurons (Fig. 4, L to N, and fig. S13, H to L).

Self-tuning adaptation of neuronal activity as a homeostatic plasticity concept was first described in primary neuronal culture (*27*) and further observed in in vivo animal models (*28*, *29*). Evidence shows that homeostatic plasticity plays a fundamental role in stabilizing neuronal activity in response to excessive perturbations under both physiological (*30*, *31*) and disease (*32*) conditions. We observed that resilient mice displayed enhanced I_h current in VTA DA neurons and simultaneously exhibited up-regulated inhibitory K^+ currents. Based on this unexpected observation, we tested the hypothesis that the resilience phenotype achieves its stable behavioral functioning through homeostatic plasticity and that this homeostatic adaptation can be established therapeutically in susceptible mice. Using pharmacological, viral, and optogenetic approaches, we found that enhancement of I_h or excessive activation of VTA DA neurons triggered self-tuning compensation of K^+ currents and functionally normalized the firing of these hyperactive neurons in susceptible animals, a homeostatic plasticity seen in VTA-NAc projections, but not in the VTA-mPFC pathway. Once the homeostatic balance is established naturally or experimentally in VTA DA neurons, these neurons are more stable, as indicated by their reduced response to physiological perturbation. Our findings advance the understanding of homeostatic plasticity in a behaviorally relevant in vivo disease

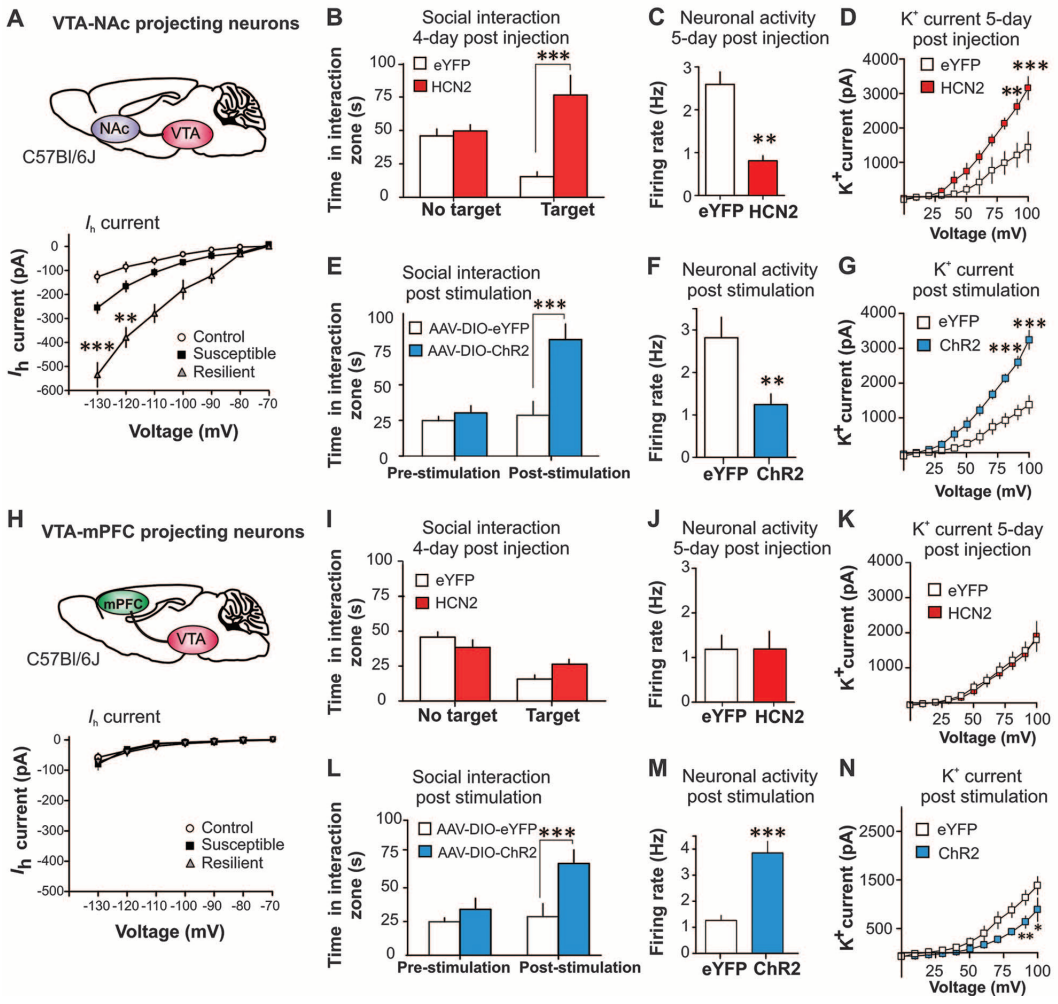

Fig. 4. The observed homeostatic plasticity is specific in the I_h-presenting VTA-NAc projection. (**A**) Statistical data of I_h in NAc-projecting VTA (VTA-NAc) neurons in control, susceptible and resilient mice. At −130 mV, $F_{(2,22)} = 39.27$, $P < 0.0001$; at −120 mV, $F_{(2,22)} = 27.78$, $P < 0.0001$; $n = 7$ to 10 cells from 6 to 7 mice per group. Post hoc analysis at −130 shows a significant increase in I_h in susceptible mice ($t_{16} = 3.98$, $P < 0.01$) and an even significantly larger I_h increase in the resilient subgroup ($t_{13} = 7.71$, $P < 0.001$), compared with the control group. (**B**) Susceptible mice expressing HCN2 in VTA-NAc neurons show an increase in social interaction ($t_{13} = 4.81$, $P < 0.001$; $n = 7$ to 8) and (**C**) a decrease in the firing rate of VTA-NAc neurons ($t_{22} = 3.31$, $P < 0.01$; $n = 11$ to 13 cells from 6 mice per group) compared with eYFP. (**D**) K^+ currents: peak (at +20 mV: $t_{12} = 4.47$, $P < 0.001$; at +10 mV: $t_{12} = 4.33$, $P < 0.01$; $n = 7$ cells from 6 mice per group). (**E**) After 5 days (20 min/day) of optical phasic stimulation of VTA-NAc neurons, susceptible animals expressing ChR2 have increased social interaction ($t_{18} = 4.24$, $P < 0.001$, $n = 10$) and (**F**) a decrease in the firing of VTA-NAc neurons expressing ChR2 ($t_{19} = 3.44$, $P < 0.01$, $n = 10$ to 11 cell from 5 to 6 mice per group). (**G**) K^+ currents are significantly increased in ChR2-expressing neurons: peak (at +20 mV: $t_{12} = 4.70$, $P < 0.001$; at +10 mV: $t_{12} = 4.82$, $P < 0.001$; $n = 7$ cells from 6 mice per group). (**H**) Statistical data of I_h in mPFC-projecting VTA (VTA-mPFC) neurons in control, susceptible, and resilient mice. At −130 mV, $F_{(2,38)} = 0.69$, $P = 0.51$; $n = 9$ to 11 cells from 5 to 6 mice per group. Susceptible mice expressing HCN2 or control eYFP in VTA-mPFC show no change in (**I**) social interaction ($t_{18} = 1.65$, $P = 0.12$; $n = 10$); (**J**) firing rate of VTA-mPFC neurons ($t_{24} = 0.34$, $P = 0.74$; $n = 13$ cells, 5 to 6 mice per group); and (**K**) K^+ currents of VTA-mPFC neurons: peak (at +20 mV: $t_{14} = 0.12$, $P = 0.90$; at +10 mV: $t_{14} = 0.85$, $P = 0.41$; $n = 8$ cells from 6 mice per group). After 5 days (20 min/day) of optical phasic stimulation of VTA-mPFC neurons, susceptible animals expressing ChR2 have increased (**L**) social interaction ($t_{18} = 4.07$, $P < 0.001$, $n = 10$) and (**M**) an increase in the firing of VTA-mPFC neurons ($t_{24} = 5.11$, $P < 0.0001$, $n = 12$ to 14 cell/group, 6 mice per group). (**N**) K^+ currents are significantly decreased after chronic activation: peak (at +20 mV: $t_{14} = 2.26$, $P < 0.05$; at +10 mV: $t_{14} = 3.20$, $P < 0.01$; $n = 8$ cells, 6 mice per group). Error bars, ±SEM. *$P < 0.05$, **$P < 0.01$, ***$P < 0.001$.

model of depression and provide further insight into the stabilized physiological underpinnings of natural resilience.

Although homeostatic plasticity describes much of our current findings, the counterintuitive process by which ionic, cellular, and behavioral alterations are achieved and its close similarity to natural stress-resilience remains surprising. Recently, cell type–specific and neural circuit–probing optogenetic approaches have assisted in unraveling multiple unforeseen functions of the brain's reward DA neurons (*9*, *11*, *22*, *23*, *26*, *33*). By revealing a previously uncharacterized ionic mechanism of intrinsic homeostatic plasticity, we are bringing new insight to the complex functions of these neurons. Notably, the experimentally induced homeostatic plasticity in VTA-NAc–projecting neurons is triggered by enhancing stress-activated I_h current and stress-induced neuronal hyperactivity. Therefore, rather than reversing the underlying disruption or pathological mechanisms, the stress-activated pathogenic changes can be beneficially used to achieve treatment efficacy (fig. S14). It is interesting that reversing pathological adaptations rapidly induces antidepressant effects (*9*, *11*), whereas chronic manipulations are needed to promote active resilient mechanisms and to achieve treatment efficacy. Overall, our findings not only unravel a critical self-stabilizing capacity of midbrain DA neurons in the brain's reward circuit, but also identify a conceptually different therapeutic strategy of promoting natural resilience. This may provide useful information for the development of naturally acting antidepressants.

References and Notes

1. V. Krishnan *et al.*, *Cell* **131**, 391–404 (2007).
2. A. Feder, E. J. Nestler, D. S. Charney, *Nat. Rev. Neurosci.* **10**, 446–457 (2009).
3. S. J. Russo, J. W. Murrough, M. H. Han, D. S. Charney, E. J. Nestler, *Nat. Neurosci.* **15**, 1475–1484 (2012).
4. S. Kumar, G. Feldman, A. Hayes, *Cognit. Ther. Res.* **32**, 734–744 (2008).
5. T. A. Carey, *Clin. Psychol. Rev.* **31**, 236–248 (2011).
6. S. M. Southwick, D. S. Charney, *Science* **338**, 79–82 (2012).
7. V. Vialou *et al.*, *Nat. Neurosci.* **13**, 745–752 (2010).
8. E. J. Nestler, W. A. Carlezon Jr., *Biol. Psychiatry* **59**, 1151–1159 (2006).
9. D. Chaudhury *et al.*, *Nature* **493**, 532–536 (2013).
10. O. Berton *et al.*, *Science* **311**, 864–868 (2006).
11. K. M. Tye *et al.*, *Nature* **493**, 537–541 (2013).
12. J.-L. Cao *et al.*, *J. Neurosci.* **30**, 16453–16458 (2010).
13. S. A. Golden, H. E. Covington 3rd, O. Berton, S. J. Russo, *Nat. Protoc.* **6**, 1183–1191 (2011).
14. M. J. Wanat, F. W. Hopf, G. D. Stuber, P. E. M. Phillips, A. Bonci, *J. Physiol.* **586**, 2157–2170 (2008).
15. H. Neuhoff, A. Neu, B. Liss, J. Roeper, *J. Neurosci.* **22**, 1290–1302 (2002).
16. N. P. Poolos, M. Migliore, D. Johnston, *Nat. Neurosci.* **5**, 767–774 (2002).
17. M. A. Frye, *N. Engl. J. Med.* **364**, 51–59 (2011).
18. M. B. Wilkinson *et al.*, *J. Neurosci.* **31**, 9084–9092 (2011).
19. Y. Nakatani, H. Masuko, T. Amano, *J. Pharmacol. Sci.* **123**, 203–206 (2013).
20. M. Biel, C. Wahl-Schott, S. Michalakis, X. Zong, *Physiol. Rev.* **89**, 847–885 (2009).
21. J. Zhang, M. S. Shapiro, *Neuron* **76**, 1133–1146 (2012).
22. H. C. Tsai *et al.*, *Science* **324**, 1080–1084 (2009).
23. J. J. Walsh *et al.*, *Nat. Neurosci.* **17**, 27–29 (2014).
24. J. W. Koo *et al.*, *Science* **338**, 124–128 (2012).
25. E. B. Margolis, J. M. Mitchell, J. Ishikawa, G. O. Hjelmstad, H. L. Fields, *J. Neurosci.* **28**, 8908–8913 (2008).
26. S. Lammel *et al.*, *Neuron* **57**, 760–773 (2008).
27. G. Turrigiano, L. F. Abbott, E. Marder, *Science* **264**, 974–977 (1994).
28. G. Turrigiano, *Annu. Rev. Neurosci.* **34**, 89–103 (2011).
29. A. Maffei, K. Nataraj, S. B. Nelson, G. G. Turrigiano, *Nature* **443**, 81–84 (2006).
30. A. Destexhe, E. Marder, *Nature* **431**, 789–795 (2004).
31. K. Whalley, *Nat. Rev. Neurosci.* **14**, 820–821 (2013).
32. D. K. Dickman, G. W. Davis, *Science* **326**, 1127–1130 (2009).
33. S. Lammel *et al.*, *Nature* **491**, 212–217 (2012).

Acknowledgments: We thank E. J. Nestler for his continuing support of this work. We also thank S. J. Russo, H. P. Xu, J. L. Cao, F. Henn, and E. J. Nestler for their helpful discussion and G. R. Tibbs and P. A. Goldstein from Weill Cornell Medical College for providing the HCN2 plasmid. This work was supported by the National Institute of Mental Health (R01 MH092306: S.M.K., D.C., M.-H.H.), National Research Service Award (F31 MH095425 to J.J.W.; T32 MH 087004 to B.J.; F32 MH096464 to A.K.F.), and Johnson & Johnson–International Mental Health Research Organization (IMHRO) Rising Star Translational Research Award (M.-H.H.).

Supplementary Materials

www.sciencemag.org/content/344/6181/313/suppl/DC1
Materials and Methods
Figs. S1 to S14
References (*34*)

3 December 2013; accepted 26 March 2014
10.1126/science.1249240

Distinct Profiles of Myelin Distribution Along Single Axons of Pyramidal Neurons in the Neocortex

Giulio Srubek Tomassy,[1] Daniel R. Berger,[2,3] Hsu-Hsin Chen,[1] Narayanan Kasthuri,[2] Kenneth J. Hayworth,[2] Alessandro Vercelli,[4] H. Sebastian Seung,[3]* Jeff W. Lichtman,[2] Paola Arlotta[1]†

Myelin is a defining feature of the vertebrate nervous system. Variability in the thickness of the myelin envelope is a structural feature affecting the conduction of neuronal signals. Conversely, the distribution of myelinated tracts along the length of axons has been assumed to be uniform. Here, we traced high-throughput electron microscopy reconstructions of single axons of pyramidal neurons in the mouse neocortex and built high-resolution maps of myelination. We find that individual neurons have distinct longitudinal distribution of myelin. Neurons in the superficial layers displayed the most diversified profiles, including a new pattern where myelinated segments are interspersed with long, unmyelinated tracts. Our data indicate that the profile of longitudinal distribution of myelin is an integral feature of neuronal identity and may have evolved as a strategy to modulate long-distance communication in the neocortex.

Myelin plays critical roles in enabling complex neuronal function, including learning and cognition, and abnormal myelination is associated with neurological disorders and mental illnesses (*1*, *2*). Given the importance of myelin for network behavior, realistic models of structure-function relations in the central nervous system (CNS) must be built in consideration of myelin structure and distribution as fundamental elements. Among all myelinated axons, the thickness of the myelin sheath varies greatly, and it is a major determinant of the speed of impulse propagation (*1*). However, structural features other than myelin thickness have the potential to contribute to establishing and modulating conduction velocity and network behavior. In particular, the alternating sequence of nodes and internodes along each axon could affect conduction speed.

High-resolution maps of myelin distribution along individual axons are not currently available. Furthermore, it is not known whether different neurons are endowed with signature patterns of longitudinal myelination. This analysis has been hampered by the technical difficulty of tracing single, long, winding axons through the complex milieu of the CNS, a task that requires electron microscopy (EM) serial reconstructions of large volumes of tissue. Fortunately, however, large EM data sets that allow analysis of myelin are beginning to be available (*3*, *4*). Here, using the neocortex as a prominent model of neuronal diversity, we traced the distribution of myelin along a large set of individual pyramidal neuron axons

[1]Department of Stem Cell and Regenerative Biology, Harvard University, 7 Divinity Avenue, Cambridge, MA 02138, USA. [2]Department of Molecular and Cellular Biology, Harvard University, 52 Oxford Street, Cambridge, MA 02138, USA. [3]Department of Brain and Cognitive Sciences, Massachusetts Institute of Technology, 43 Vassar Street, Cambridge, MA 02139, USA. [4]Neuroscience Institute Cavalieri Ottolenghi, Neuroscience Institute of Turin, Corso M. d'Azeglio 52, 10126 Turin, Italy.

*Present address: Princeton Neuroscience Institute, Princeton University, Princeton, NJ 08544, USA.
†Corresponding author. E-mail: paola_arlotta@harvard.edu

www.sciencemag.org/content/344/6181/313/suppl/DC1

Supplementary Materials for

Enhancing Depression Mechanisms in Midbrain Dopamine Neurons Achieves Homeostatic Resilience

Allyson K. Friedman, Jessica J. Walsh, Barbara Juarez, Stacy M. Ku, Dipesh Chaudhury, Jing Wang, Xianting Li, David M. Dietz, Nina Pan, Vincent F. Vialou, Rachael L. Neve, Zhenyu Yue, Ming-Hu Han*

*Corresponding author. E-mail: ming-hu.han@mssm.edu

Published 18 April 2014, *Science* **344**, 313 (2014)
DOI: 10.1126/science.1249240

This PDF file includes

Materials and Methods

Chronic social defeat and social interaction**.**

Chronic social defeat and avoidance testing were performed according to published protocols and our previous work (*1, 9, 10, 13*). During each defeat episode, male tyrosine hydroxylase TH-GFP or TH-Cre C57BL/6J 8 week old mice were exposed to a 10 min physical bout of interaction with an aggressive CD1 mouse. For the remainder of the time the C57 mouse is housed across a clear plexiglass divider providing further stressful sensory cues from the CD1 mouse. After the 10-day social defeat the C57 is singly housed. 24 hr following defeat the C57 undergoes a social interaction test with a novel CD1 aggressor. The social interaction test, measured the time spent in the interaction zone during the first (target absent) and second (target present) trials; the interaction ratio (IR) was calculated as 100 x [(interaction time, target present)/(interaction time, target absent)]. Behavioral phenotyping on days 11 and following re-test were performed. Defeated mice with IR<100 were defined as susceptible mice; other defeated mice are used as the resilient subgroup.

Electrophysiology.

All recordings were carried out blind to the experimental conditions of behavioral, drug and viral treatment. Acute brain slices of VTA were prepared as done in previous studies (*9, 12, 24, 34*). Male TH-GFP, TH-Cre or C57BL/6J 11-15 week old mice were perfused with cold artificial cerebrospinal fluid (aCSF) containing (in mM): 128 NaCl, 3 KCl, 1.25 NaH_2PO_4, 10 D-glucose, 24 $NaHCO_3$, 2 $CaCl_2$, and 2 $MgCl_2$ (oxygenated with 95% O_2 and 5% CO_2, pH 7.35, 295–305 mOsm). Acute brain slices (250 μm) containing the VTA were cut using a microslicer in sucrose-ACSF, which was derived by fully replacing NaCl with 254 mM sucrose, and saturated by 95% O_2 and 5% CO_2. Slices were maintained in the holding chamber for 1 hr at 37°C. Slices were transferred into a recording chamber fitted with a constant flow rate of aCSF equilibrated with 95% O_2/5% CO_2 (2.5 ml/min) and at 35°C. Glass microelectrodes (2-4 MΩ) filled with an internal solution containing (mM): 115 potassium gluconate, 20 KCl, 1.5 $MgCl_2$, 10 phosphocreatine, 10 HEPES, 2 magnesium ATP, and 0.5 GTP (pH 7.2, 285 mOsm). VTA DA neurons were identified by their location and infrared differential interference contrast microscopy and recordings were made from TH-GFP positive neurons, eYFP

positive neurons for viral and optogenetic experiments and lumafluor positive neurons for projection-specific recordings (Fig. 1 to 4) (*9*). Electrophysiological properties were evaluated from whole-cell recordings as shown in fig. S2. Duration was determined from half amplitude from threshold to peak. Firing rate was recorded with cell-attached configuration (*1, 9*). Whole-cell voltage-clamp was used to record I_h current with a series of 3 s pulses with 10 mV command voltage steps from –130 mV to –70 mV from a holding potential at –70 mV (*12*). To isolate voltage-gated K^+ channel-mediated currents, 4 s pulses with 10 mV step voltages from –70 to +20 at –70 holding potential were used in the presence of aCSF containing 1 μM tetrodotoxin, 200 μM $CdCl_2$, 1mM kynurenic acid, and 100 μM picrotoxin as performed in our previous study (*24, 34*). Cell excitability was measured with 2 s incremental steps of current injections (50, 100, 150, and 200 pA) (*9*). Series resistance was monitored during all recordings.

Cannula surgery and micro-infusion of lamotrigine into the VTA.

24 hr after social interaction test mice were placed under a combination of ketamine (100 mg/kg)/xylazine (10 mg/kg) anesthesia before bilateral stereotaxic implantation of 26 gauge guide cannula fitted with obturators that were secured to the skull after being positioned 1 mm directly above the VTA (AP, −3.2; ML, 0.4; DV, −3.7 mm; 0° angle) as described previously (*9, 12*). After 5 days of postoperative recovery, simultaneous bilateral microinjections of lamotrigine (0.1 μg) or vehicle (phosphate-buffered saline, PBS) was delivered through an injector cannula in a total volume 0.4 μl/side at a continuous rate of 0.1 μl/min under the control of a micro-infusion pump. Concentration was selected based on published studies and on validation of *in vitro* effects on DA neuron activity in this study (*16*). Injector cannulas were removed 5 min after the stopping of each infusion to prevent backflow. Cannula placements were confirmed postmortem in all animals.

Sucrose preference.

For two-bottle choice sucrose-preference testing, a solution of 1% sucrose or drinking water was filled in two 50 ml tubes with stoppers fitted with ball-point sipper tubes as described previously (*1, 9*). All animals were singly housed and acclimatized to two-bottle choice conditions prior to testing conditions. 12 hr or 24 hr post treatment, fluid

was weighed and the positions of the tubes were interchanged. Sucrose preference was calculated as a percentage [100 × (volume of sucrose consumed (in bottle A)/total volume consumed (bottles A and B))].

Forced swim test.

The forced swim test (FST) was performed as previously described (*7*). 4 days post viral injection or 24 hour post optogenetic stimulation mice were placed for 6min in a 4 liter Pyrex glass beaker containing 3 liters of water at 24±1°C. Water was changed between subjects. All test sessions were recorded by a digitally tracking Ethovision positioned on the side of the beaker. Time spent immobile was independently analyzed by Ethovision software. A decrease in immobility time indicates an antidepressant-like response (*7*).

Immunohistochemistry.

Mice were fully anesthetized with ketamine (100mg/kg) with xylazine (10mg/ml) mixture before the vascular perfusion as described previously (*1,9*). Mice were perfused with 30ml cold PBS and 30ml 4% paraformaldehyde (PFA). Brain tissue were removed and post-fixed with 4% PFA, then treated with 30% sucrose at 4^{o}C for two days. The VTA region of the brain were sliced on the cryostat, the sections were collected consecutively and preserved into antifreeze buffer (30% Glycerin solution in ethylene glycol) at –20 ºC. Brain tissue was sectioned with thickness of 30µm and sections were stored in 4 ºC in PBS and sodium azide until IHC. For immuno-staining and quantification of VTA DA neurons, serial sections representing the rostral to caudal extent of the VTA were selected for analysis. Brain sections were rinsed 3X with PBS and blocked with blocking buffer (5% goat serum, PBS with 0.2@ Triton X-100) for 1 hr. Sections were incubated with primary Anti-TH (Sigma, 1:10,000)and anti-GFP (Invitrogen, 1:2000) monoclonal antibody at 4 ºC for 24 hr. The next day sections were incubated with secondary antibody (Alexa Fluor 488, Goat x mouse IgG) for 2 hr. Sections were then rinsed with PBS 3 times before mounting on the slide (*9, 24*). Sections were subsequently imaged (×20 magnification) on a LSM 710 confocal (Zeiss). Cell counting was carried out manually using ImageJ.

Virus vectors.

AAV-DIO-ChR2-eYFP and AAV-DIO-eYFP virus plasmids were purchased from University of North Carolina vector core facility (UNC). HSV-LS1L-HCN2-eYFP and

HSV-LS1L-eYFP were provided by Rachael Neve's laboratory in Massachusetts Institute of Technology (MIT). An AAV2/5 vector that undergoes retrograde transport, expressing Cre (AAV2/5-Cre) was used in this study for targeting VTA-NAc pathway and VTA-mPFC pathway, respectively. The vector was purchased from University of Pennsylvania Vector Core.

Stereotaxic surgery, viral-mediated gene transfer, and optic fiber placement.

The related procedures were performed as described previously (*9, 23, 24*). TH-Cre mice were anesthetized with ketamine (100 mg/kg)/xylaxine (10 mg/kg) mixture, placed in a stereotaxic apparatus and their skull was exposed by scalpel incision. For viruses, thirty-three gauge needles were placed bilaterally at 7^{o} angle into the VTA (AP –3.3; LM +1.0; DV –4.6 in the mm) and 0.5 μl of virus was infused at a rate of 0.1 μl/min as performed in our previous study (*9, 23, 24*). We utilized the chronic implantable optical fiber system as performed in our previous studies (*9, 23*). Chronically implantable fibers were made with 200 μm core optic fiber and light output through the optical fibers was measured prior to bilateral implantation. Fibers measuring at least 10 mW were utilized. They were implanted into the VTA at a 7^{o} angle (AP –3.3 mm; LM +1.0 mm; DV –4.4 mm) and secured to the skull with industrial strength dental cement. Implantable optical fibers ensure that the same tissue is repeatedly stimulated. Optical fiber placements were confirmed postmortem in all animals.

Projection-specific manipulations.

To selectively target either the NAc or mPFC projecting VTA neurons we used a combination of a retrograding AAV2/5-Cre injected in to either site, and Cre inducible virus AAV-DIO-ChR2-eYFP or HSV-LS1L-HCN2-eYFP injected into the VTA. Retrograding AAV2/5-Cre was injected to the NAc (bregma coordinates: AP, +1.5; LM, +1.6; DV, –4.4; 10° angle) or mPFC (bregma coordinates: AP, +1.7; LM, +1.6; DV, –2.5; 15° angle), and Cre-inducible AAV-DIO-ChR2-eYFP or HSV-LS1L-HCN2-eYFP to the VTA. Therefore, ChR2 or HCN2 was expressed selectively in NAc or mPFC projecting neurons in the VTA.

Blue light stimulation.

To selectively activate the DA neurons in the VTA, cell-type specific expression of ChR2 was realized by combined use of TH-Cre mice and Cre-inducible AAV-DIO-ChR2-eYFP

(University of North Carolina). While this viral vector and mouse line were successfully used in our previous work (*9, 23*), morphological and functional validations were further performed in this study. 473 nm blue laser diode and a stimulator were used to generate blue light pulses as described previously (*9, 23*). For *in vitro* slice electrophysiological validation of ChR2 activation we tested 0.1–50 Hz stimulation protocols. For all *in vivo* behavioral experiments, mice were given, high frequency, phasic (20 Hz, 40 ms; 80% duty cycle) light stimulations (*9*). This protocol was established based on *in vivo* studies that showed an increase in overall firing as well as burst firing in VTA DA neurons in susceptible animals (*12*).

Statistics.

Unless otherwise noted, we used two-tailed unpaired Student's t tests (for comparison of two groups), one-way analysis of variance (ANOVA) followed by *t*-test comparison (for three groups).

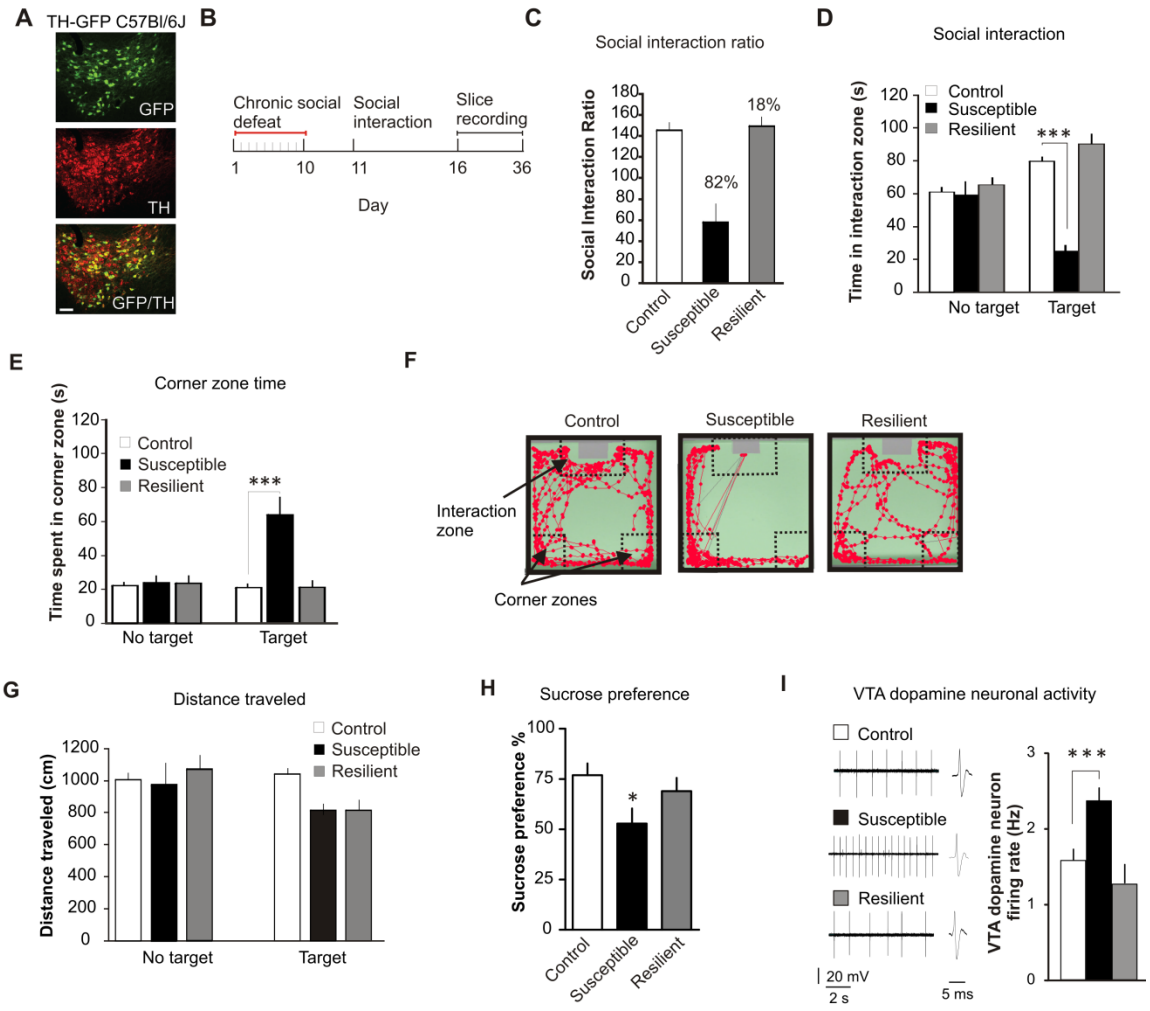

Fig. S1. Determination, distribution and behavior of susceptible and resilient subgroups following 10-day social defeat paradigm. (**A**) Confocal image of immuno-staining for TH in TH-GFP mice. Quantification shows: 72.3% ± 2.15 of VTA neurons were TH^+, 54.2% ± 6.22% were $eYFP^+$, and 97 % ± 1.0 % of the TH neurons were also labeled with eYFP (2–3 sections per mouse; data from 5 animals). Scale bar, 100 µm; green, GFP; red, TH. (**B**) Experimental timeline. (**C**) Social interaction ratio, and percentage breakdown of mice in either susceptible or resilient subgroup. (**D**) Social interaction time ($F_{(2,53)}$ = 107.87, $P < 0.0001$, n = control:30, susceptible:14, resilient:10). (**E**) Time spent in corner zone during social interaction test is significantly increased in susceptible mice ($F_{(2,53)}$ = 21.10, $P < 0.0001$; n = control:30, susceptible:14, resilient:10). (**F**) Representative traces of mouse behavior during social interaction test after having undergone chronic social defeat 24 hr earlier. (**G**) Distance traveled is not significantly different between phenotypes ($F_{(2,53)}$ = 0.26, P = 0.77; n = control:30, susceptible:14, resilient:10). (**H**) Sucrose preference is significantly reduced in the susceptible subgroup compared to control and resilient ($F_{(2,35)}$ = 3.42, $P < 0.05$; n = 12). (**I**) Baseline DA neuron firing frequency of VTA brain slices from TH-GFP control, susceptible and resilient mice after chronic (10-day) social defeat ($F_{(2,37)}$ = 7.24, $P < 0.001$, n = 12–14). Error bars, ± SEM. * $P < 0.05$, *** $P < 0.001$.

Comparison of electrophysiological properties

	Membrane potential (mV)	Threshold (mV)	Peak (mV)	Duration (ms)	Afterhyperpolarizations (mV)
□ Control	-55.4 ± 0.85	-37.7 ± 1.0	16.4 ± 6.5	0.76 ± 0.03	-63.7 ± 2.8
■ Susceptible	-56.6 ± 0.89	-36.4 ± 1.2	16.6 ± 4.3	0.75 ± 0.06	-64.6 ± 1.9
■ Resilient	-55.5 ± 1.22	-37.9 ± 1.1	15.5 ± 6.2	0.76 ± 0.05	-63.9 ± 1.6

Fig. S2. Control, susceptible and resilient VTA GFP $^{+}$ DA neurons show no significantly different electrophysiological properties. Membrane potential: $F_{(2,74)} = 0.48$, $P = 0.62$; Action potential threshold: $F_{(2,74)} = 0.98$, $P = 0.38$; Action potential peak: $F_{(2,74)} = 0.16$, $P = 0.85$; Action potential duration $F_{(2,74)} = 1.93$, $P = 0.15$; Afterhyperpolarization $F_{(2,74)} = 0.94$, $P = 0.40$. (n = 25 cells/ 5 mice per group).

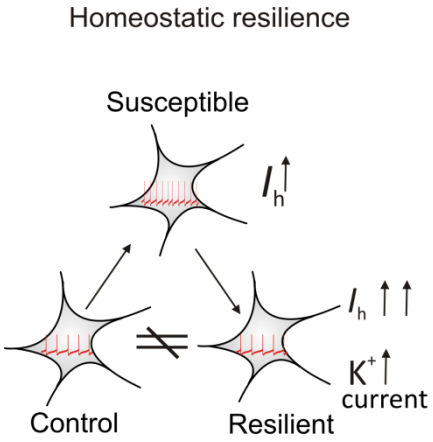

Fig. S3. Schematic model summary of behavioral, physiological and ionic findings. The resilient phenotype shows control-level activity of VTA dopamine neurons, a stabilized firing status established by a new balance of I_h and K^+ channel currents.

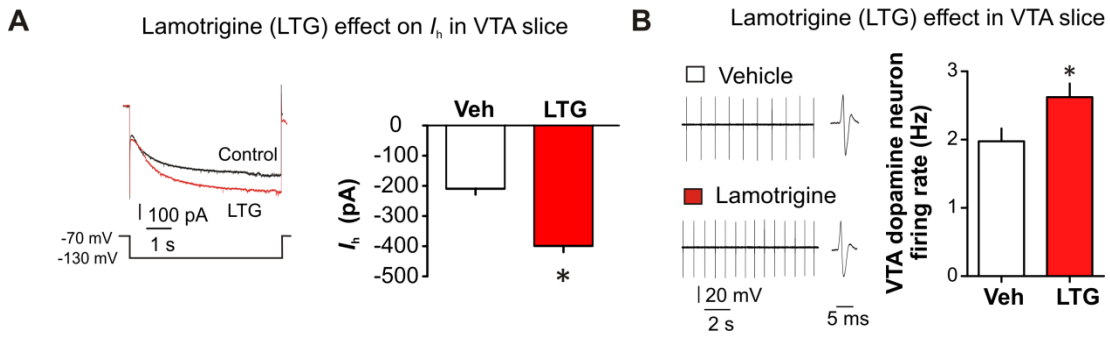

Fig. S4. Lamotrigine increases I_h current and the firing rate of VTA dopamine neurons in brain slice preparation. (**A** and **B**) Lamotrigine perfusion *in vitro* significantly increases both VTA DA neuron I_h current ($t_{13} = 2.84$, $P < 0.05$) and firing rate ($t_{13} = 2.60$, $P < 0.05$; n = 7–8). Error bars, ± SEM. * $P < 0.05$.

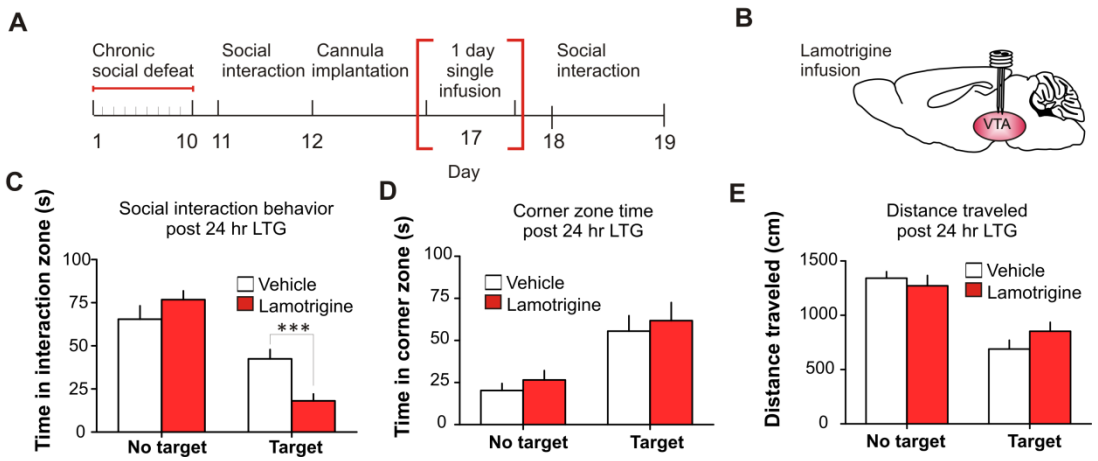

Fig. S5. A single infusion of I_h potentiator lamotrigine enhances social avoidance in susceptible mice. (**A** and **B**) Experimental timeline: following a 5 day recovery from bilateral VTA cannula surgery mice, susceptible mice received single dose infusion and behavioral testing. **(C)** Social interaction behavior post infusion of lamotrigine in susceptible mice increases social avoidance (t_{14} = 4.48, P < 0.001, n = 8). (**D**) Corner zone time is not altered (t_{14} = 0.66, P = 0.52, n = 8). (**E)** Locomotion activity is not altered post a single administration of lamotrigine or vehicle (t_{14} = 1.31, P = 0.213, n = 8). Error bars, ± SEM. *** P < 0.001.

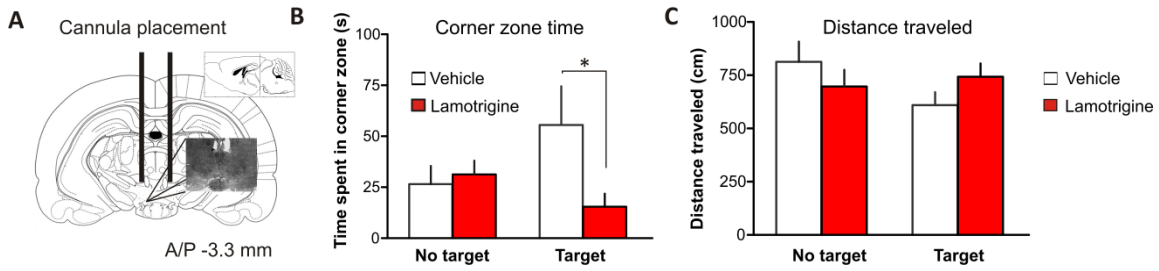

Fig. S6. Repeated infusion of lamotrigine to the VTA of susceptible animals decreases the time spent in the corner zone and does not alter distance traveled**.** (**A**) Schematic coronal sections from VTA (adapted from Allen Brain Atlas) with an inset of sample crystal violet stain of VTA bilateral cannula placement used in micro-infusion experiment. Accurate injection sites were confirmed in all animals post-mortem. (**B**) Corner zone time is decreased ($t_{18} = 2.67$, $P < 0.05$; n = 10). (**C**) Locomotor activity is not altered following chronic infusion of lamotrigine ($t_{18} = 1.71$, $P = 0.11$; n = 10). Error bars, ± SEM. * $P < 0.05$.

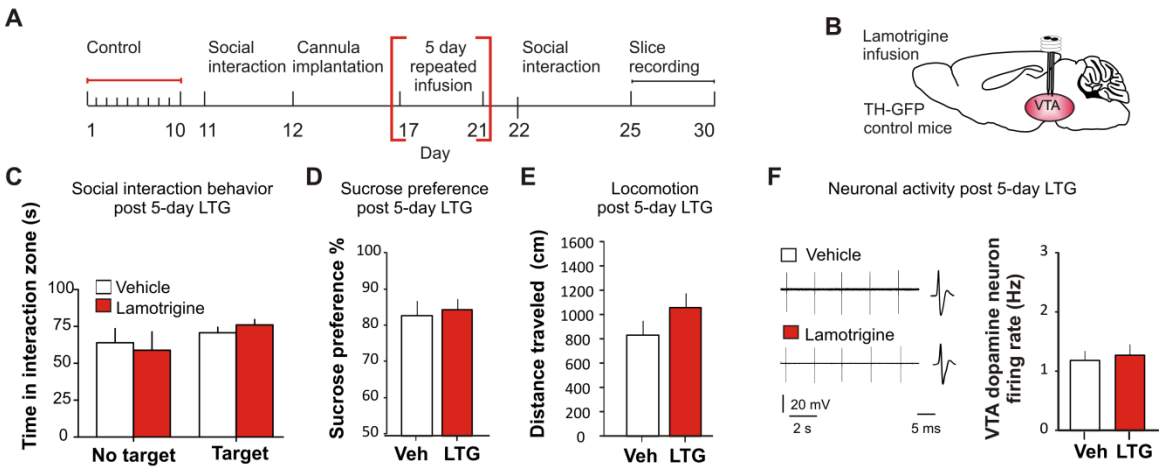

Fig. S7. Repeated infusion of I_h potentiator lamotrigine to the VTA of control mice does not alter social behavior or neuronal activity (**A**) Experimental timeline. (**B**) Schematic of lamotrigine infusion into the VTA of stress naïve control TH-GFP mice. (**C**) 5 days of 3 min daily bilateral infusions of lamotrigine (LTG, 0.1 µg) or vehicle into the VTA does not alter social interaction time ($t_{16} = 0.31$, $P = 0.76$; n = 9), (**D**) sucrose preference ($t_{16} = 0.44$, $P = 0.67$; n = 9) or (**E**) distance traveled ($t_{16} = 1.74$, $P = 0.10$; n = 9) . (**F**) Sample traces and statistic data of VTA DA neuron firing in control mice following repeated infusion of vehicle compared to lamotrigine ($t_{22} = 0.50$, $P = 0.62$; n = 12 cells/6 mice per group). Error bars, ± SEM.

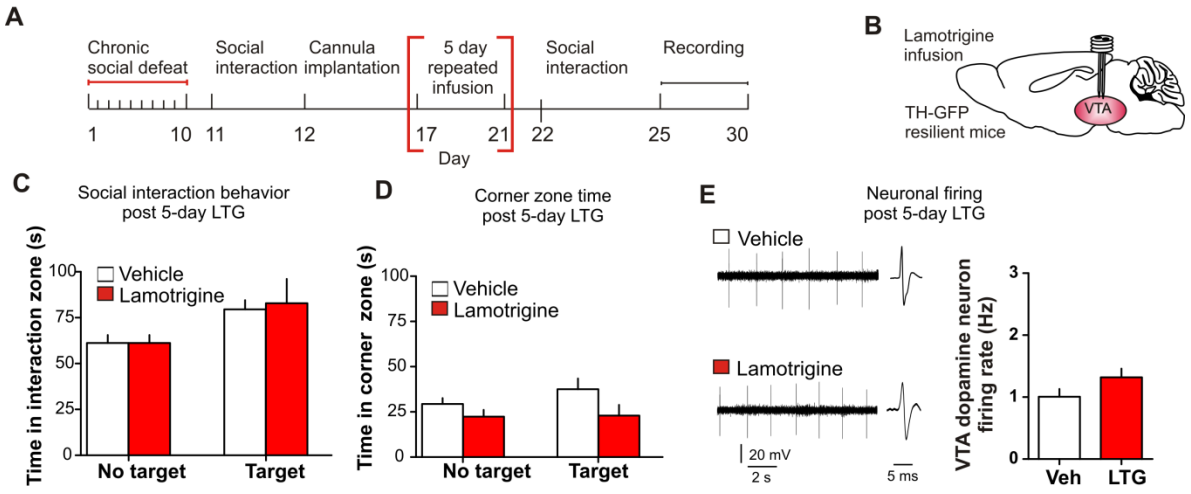

Fig. S8. Repeated infusion of I_h potentiator lamotrigine to the VTA of resilient mice does not alter social behavior or neuronal activity (**A**) Experimental timeline. (**B**) Schematic of lamotrigine infusion into the VTA of resilient TH-GFP mice. (**C**) 5 day of 3 min daily bilateral infusions of lamotrigine (0.1 µg) or vehicle into the VTA does not alter social interaction time ($t_{10} = 0.24$, $P = 0.82$; n = 6) or (**D**) corner zone time ($t_{10} = 1.74$, $P = 0.11$; n = 6) . (**E**) Sample traces and statistic data of VTA dopamine neuron firing in control mice following repeated infusion of vehicle compared to lamotrigine ($t_{46} = 1.86$, $P = 0.10$; n = 24 cells/5 mice per group). Error bars, ± SEM.

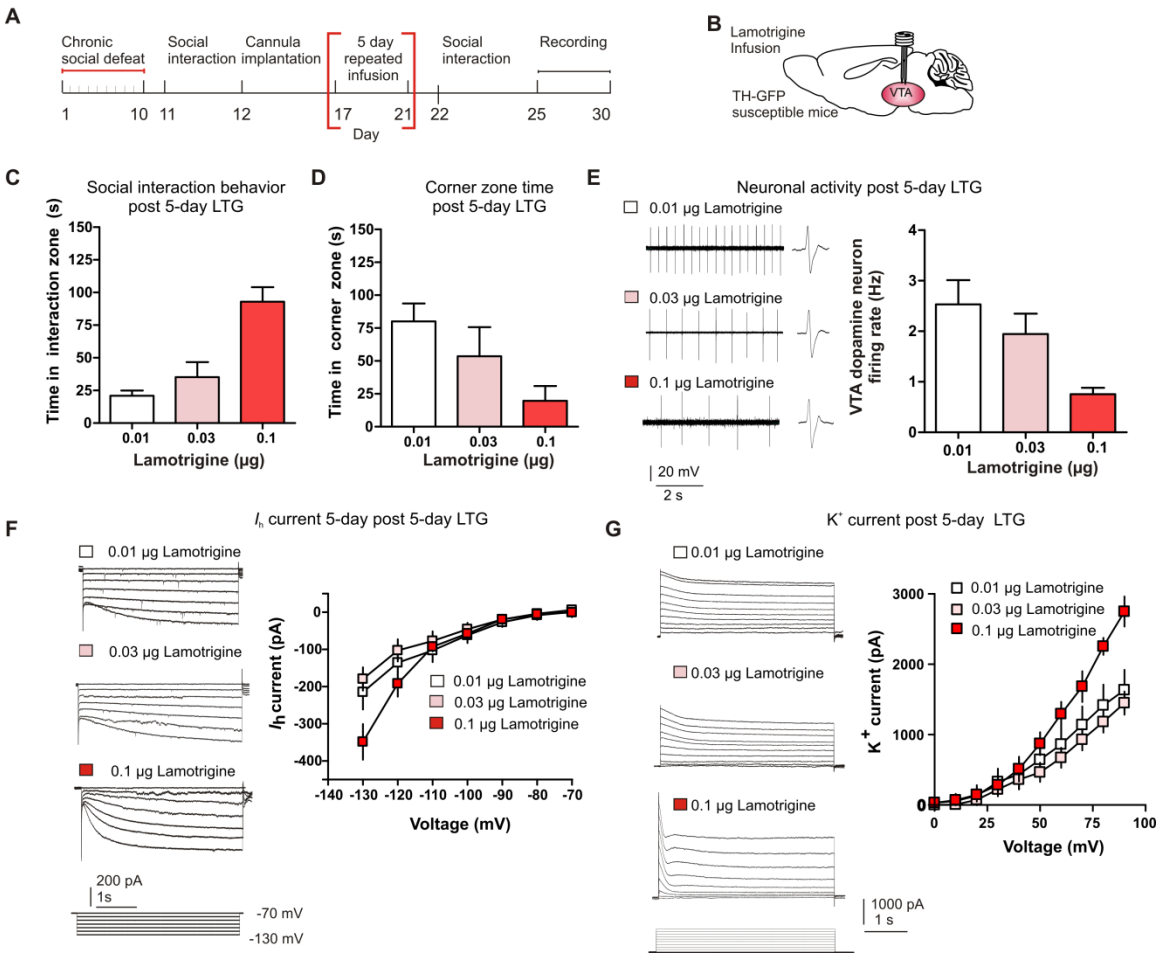

Fig. S9. Dose response of repeated lamotrigine infusion to the VTA of susceptible mice. (**A**) Experimental timeline. (**B**) Schematic of lamotrigine infusion into susceptible TH-GFP mice. (**C**) Social interaction time and (**D**) corner zone time with target following 5 day infusion of lamotrigine at 0.01 µg, 0.03 µg and 0.1 µg concentration (n = 5). (**E**) Sample traces and group data of firing rate following the 5 day infusion of lamotrigine at 0.01 µg, 0.03 µg and 0.1 µg concentrations, (n = 5 cells/ 3 animals per group). (**F**) Sample traces and group data of I_h following the 5 day infusion of lamotrigine at 0.01 µg, 0.03 µg and 0.1 µg concentrations (n = 6–7 cells/ 3 animals per group). (**G**) Sample traces and group data of K^+ channel currents following the 5 day infusion of lamotrigine at 0.01 µg, 0.03 µg and 0.1 µg concentrations (n = 5–6 cells/ 3 animals per group). Error bars, ± SEM.

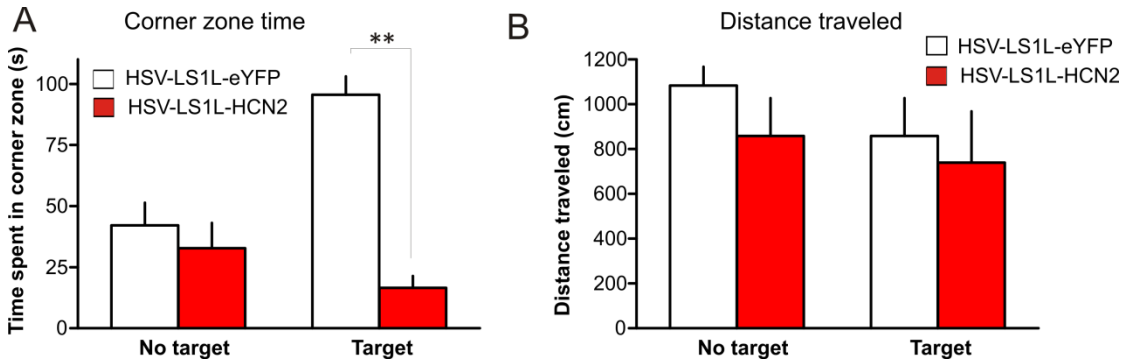

Fig. S10. Overexpression of HCN2 channels in TH^+ neurons of susceptible mice significantly reduces corner zone time and does not alter locomotor activity. (**A**) Corner zone time is decreased ($t_{18} = 4.18$, $P < 0.01$ n = 10) and (**B**) locomotor activity is not altered ($t_{18} = 0.14$ $P = 0.89$; n = 10) with target present. Error bars, ± SEM. ** $P < 0.01$.

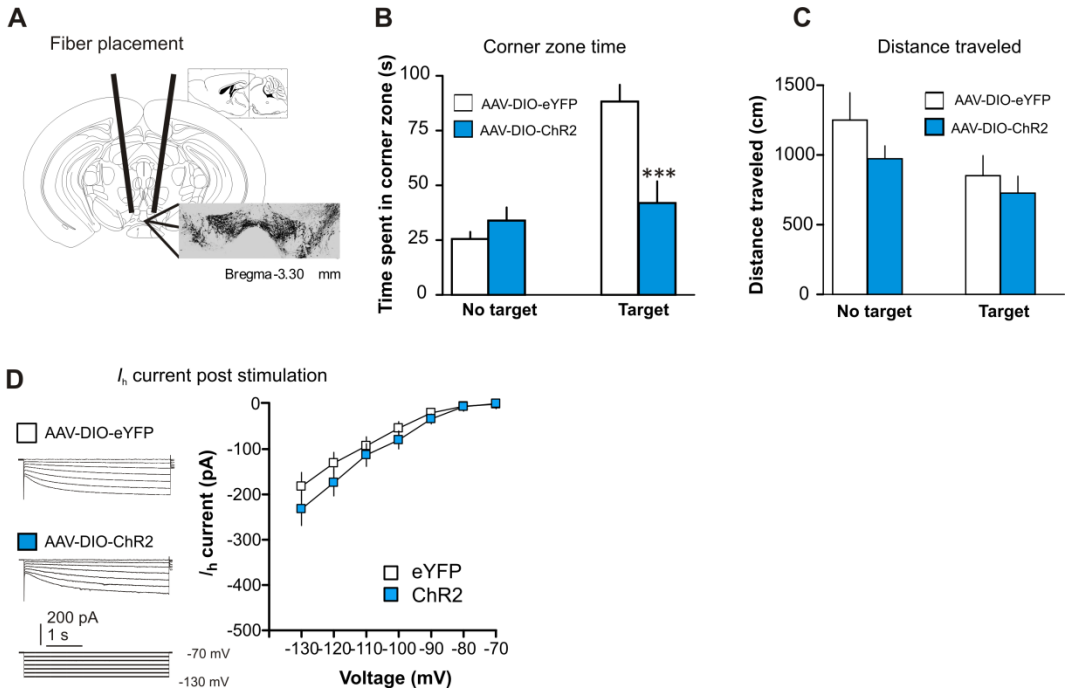

Fig. S11. Repeated optogenetic stimulation of VTA DA neurons significantly reduces corner zone time and does not alter locomotion or I_h. (**A**) Schematic coronal sections from VTA (adapted from Allen Brain Atlas) with an inset of sample crystal violet stain of VTA bilateral ferrule placement used in optogenetics experiment. Accurate stimulation sites were confirmed in all animals post mortem. (**B**) In the presence of a social target, previously susceptible mice, injected with AAV-DIO-ChR2-eYFP and given chronic photo-activation 20 minutes a day for 5 days spent significantly less time in the corner zone compared to susceptible mice injected with control AAV-DIO-eYFP ($t_{22} = 3.59$, $P < 0.001$; n = 12). (**C**) There was no difference in total distance traveled during the social interaction test ($t_{22} = 1.03$, $P = 0.32$; n = 12). (**D**) Sample traces and statistic data of I_h show no change following photo-activation (At -130 pA: $t_{27} = 1.148$, $P = 0.261$; n = 14–15 cells). Error bars, ± SEM. *** $P < 0.001$.

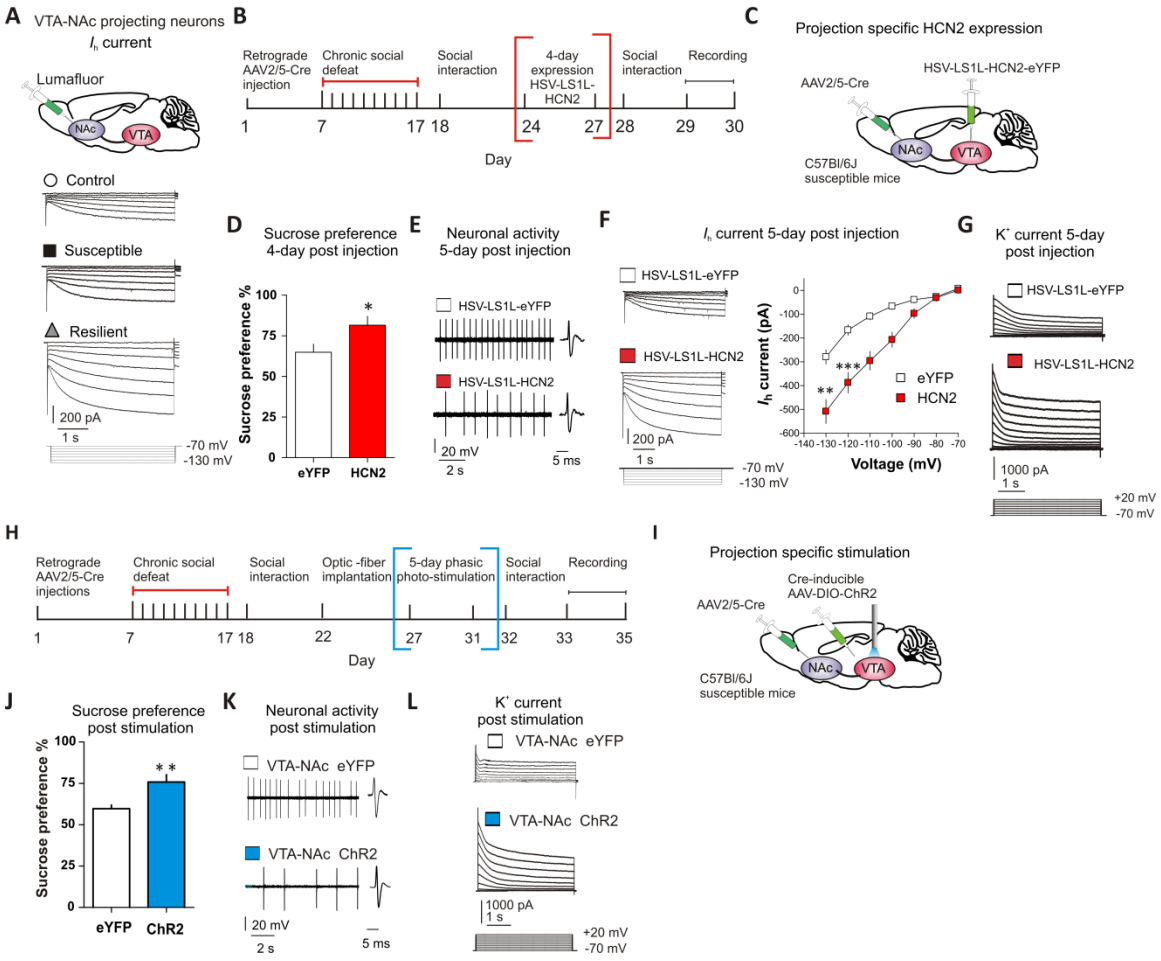

Fig. S12. The observed homeostatic plasticity is specific in I_h-presenting VTA-NAc projection. (**A**) Sample traces of I_h in VTA-NAc neurons labeled by lumafluor injection. (**B**) Experimental timeline. (**C**) Retrograding AAV2/5-Cre bilateral injection into the NAc and Cre-inducible HSV-LS1L-HCN2-eYFP bilateral injection into the VTA. (**D**) Sucrose preference test is significantly different post 4 day injection ($t_{10} = 2.25$, $P < 0.05$; n = 6). (**E**) Sample traces firing activity of VTA-NAc neurons following expression of HCN2 virus. (**F**) Sample traces and statistic data of I_h increase in VTA-NAc neurons following expression of HCN2 virus (At –130 mV: $t_{18} = 3.60$, $P < 0.01$; –120 mV: $t_{18} = 5.87$, $P < 0.0001$; n = 10 cells/6 mice per group). (**G**) Sample traces of peak K^+ current of VTA-NAc neurons following expression of HCN2 virus. (**H**) Experimental timeline. (**I**) Retrograding AAV2/5-Cre bilateral injection into the NAc and Cre-inducible AAV-DIO-ChR2 bilateral injection and optic-fiber implantation into the VTA. (**J**) Sucrose preference test is significantly different post 5 day stimulation ($t_{20} = 3.25$, $P < 0.01$; n = 11). (**K**) Sample traces of firing activity of VTA-NAc neurons post 5 day stimulation. (**L**) Sample traces of peak K^+ current of VTA projecting NAc neurons post 5 day stimulation. Error bars, ± SEM. * $P < 0.05$, ** $P < 0.01$, *** $P < 0.001$.

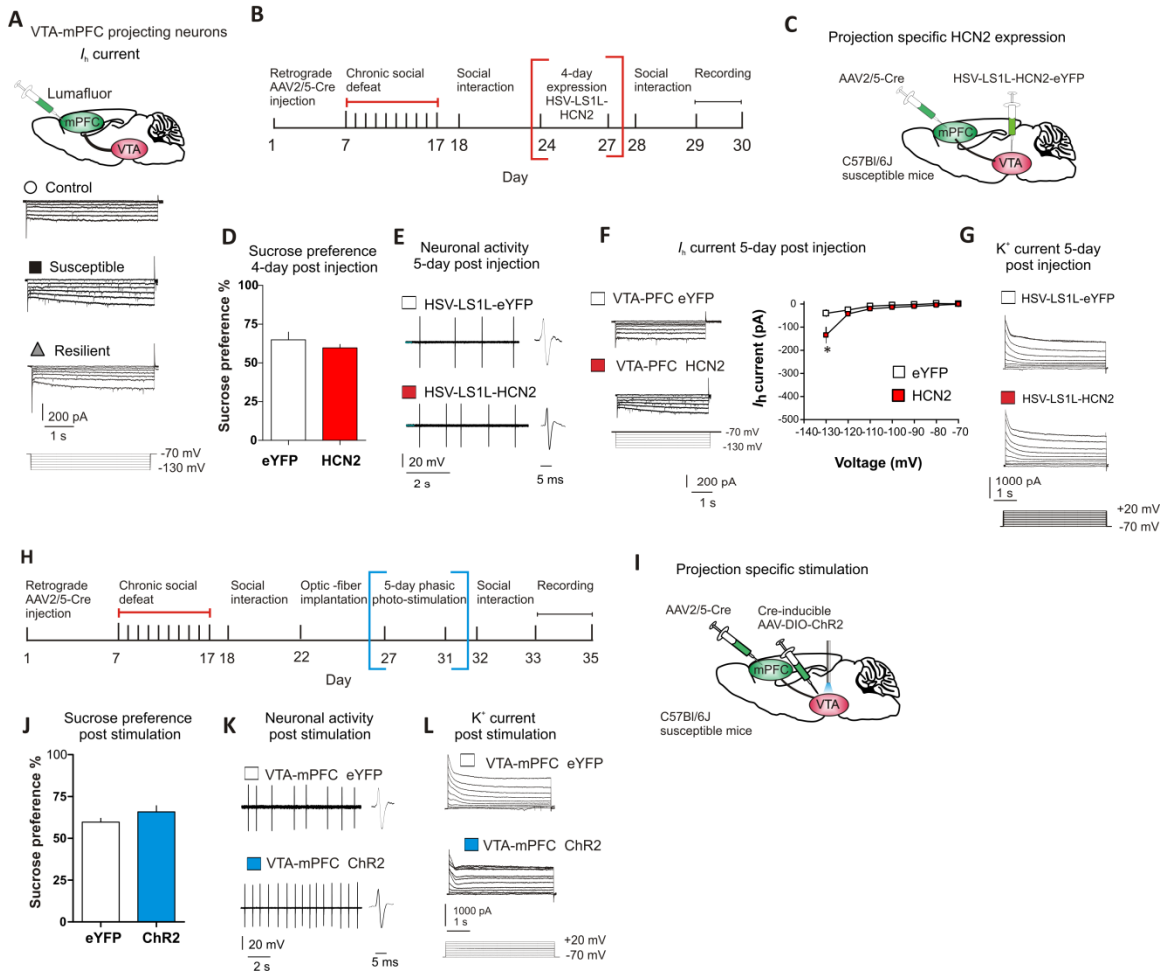

Fig. S13. mPFC projecting VTA neurons demonstrate I_h-independent plasticity. (**A**) Sample traces of I_h in VTA-mPFC neurons labeled by lumafluor injection. (**B**) Experimental timeline. (**C**) Retrograding AAV2/5-Cre bilateral injection into the mPFC and Cre-inducible HSV-LS1L-HCN2-eYFP bilateral injection into the VTA. (**D**) Sucrose preference test is not significantly different post 4 day injection ($t_{18} = 0.36$, $P = 0.72$; n = 10). (**E**) Sample traces firing activity of VTA-mPFC neurons following expression of HCN2 virus. (**F**) Sample traces and statistic data of I_h in VTA-mPFC neurons following expression of HCN2 virus (At –130 mV: $t_{18} = 2.12$, $P < 0.05$; n = 10 cells/5 mice per group). (**G**) Sample traces of peak K^+ current of VTA-mPFC neurons following expression of HCN2 virus. (**H**) Experimental timeline. (**I**) Retrograding AAV2/5-Cre bilateral injection into the mPFC and Cre-inducible AAV-DIO-ChR2 bilateral injection and optic fiber implantation into the VTA. (**J**) Sucrose preference test is not significantly different post 5 day stimulation. ($t_{20} = 1.42$, $P = 0.17$; n = 11). (**K**) Sample traces of firing activity of VTA-mPFC neurons post 5 day stimulation. (**L**) Sample traces of peak K^+ current of VTA-mPFC neurons post 5 day stimulation. Error bars, ± SEM. * $P < 0.05$.

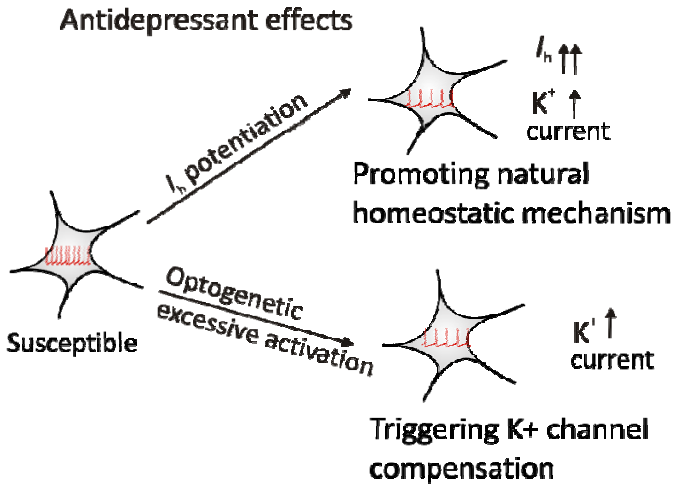

Fig. S14. Novel therapeutic strategy. Further increasing I_h in susceptible animals or excessive activation of already hyperactive VTA DA neurons subsequently induced a homeostatic compensatory up-regulation of K^+ channel-mediated currents and established a more stable neuronal status, the same phenomenon observed in resilient mice.

References

1. V. Krishnan, M. H. Han, D. L. Graham, O. Berton, W. Renthal, S. J. Russo, Q. Laplant, A. Graham, M. Lutter, D. C. Lagace, S. Ghose, R. Reister, P. Tannous, T. A. Green, R. L. Neve, S. Chakravarty, A. Kumar, A. J. Eisch, D. W. Self, F. S. Lee, C. A. Tamminga, D. C. Cooper, H. K. Gershenfeld, E. J. Nestler, Molecular adaptations underlying susceptibility and resistance to social defeat in brain reward regions. *Cell* **131**, 391–404 (2007). doi:10.1016/j.cell.2007.09.018 Medline

2. A. Feder, E. J. Nestler, D. S. Charney, Psychobiology and molecular genetics of resilience. *Nat. Rev. Neurosci.* **10**, 446–457 (2009). doi:10.1038/nrn2649 Medline

3. S. J. Russo, J. W. Murrough, M. H. Han, D. S. Charney, E. J. Nestler, Neurobiology of resilience. *Nat. Neurosci.* **15**, 1475–1484 (2012). doi:10.1038/nn.3234 Medline

4. S. Kumar, G. Feldman, A. Hayes, Changes in mindfulness and emotion regulation in an exposure-based cognitive therapy for depression. *Cognit. Ther. Res.* **32**, 734–744 (2008). doi:10.1007/s10608-008-9190-1

5. T. A. Carey, Exposure and reorganization: The what and how of effective psychotherapy. *Clin. Psychol. Rev.* **31**, 236–248 (2011). doi:10.1016/j.cpr.2010.04.004 Medline

6. S. M. Southwick, D. S. Charney, The science of resilience: Implications for the prevention and treatment of depression. *Science* **338**, 79–82 (2012). doi:10.1126/science.1222942 Medline

7. V. Vialou, A. J. Robison, Q. C. Laplant, H. E. Covington 3rd, D. M. Dietz, Y. N. Ohnishi, E. Mouzon, A. J. Rush 3rd, E. L. Watts, D. L. Wallace, S. D. Iñiguez, Y. H. Ohnishi, M. A. Steiner, B. L. Warren, V. Krishnan, C. A. Bolaños, R. L. Neve, S. Ghose, O. Berton, C. A. Tamminga, E. J. Nestler, DeltaFosB in brain reward circuits mediates resilience to stress and antidepressant responses. *Nat. Neurosci.* **13**, 745–752 (2010). doi:10.1038/nn.2551 Medline

8. E. J. Nestler, W. A. Carlezon Jr., The mesolimbic dopamine reward circuit in depression. *Biol. Psychiatry* **59**, 1151–1159 (2006). doi:10.1016/j.biopsych.2005.09.018 Medline

9. D. Chaudhury, J. J. Walsh, A. K. Friedman, B. Juarez, S. M. Ku, J. W. Koo, D. Ferguson, H. C. Tsai, L. Pomeranz, D. J. Christoffel, A. R. Nectow, M. Ekstrand, A. Domingos, M. S. Mazei-Robison, E. Mouzon, M. K. Lobo, R. L. Neve, J. M. Friedman, S. J. Russo, K. Deisseroth, E. J. Nestler, M. H. Han, Rapid regulation of depression-related behaviours by control of midbrain dopamine neurons. *Nature* **493**, 532–536 (2013). doi:10.1038/nature11713 Medline

10. O. Berton, C. A. McClung, R. J. Dileone, V. Krishnan, W. Renthal, S. J. Russo, D. Graham, N. M. Tsankova, C. A. Bolanos, M. Rios, L. M. Monteggia, D. W. Self, E. J. Nestler, Essential role of BDNF in the mesolimbic dopamine pathway in social defeat stress. *Science* **311**, 864–868 (2006). doi:10.1126/science.1120972 Medline

11. K. M. Tye, J. J. Mirzabekov, M. R. Warden, E. A. Ferenczi, H. C. Tsai, J. Finkelstein, S. Y. Kim, A. Adhikari, K. R. Thompson, A. S. Andalman, L. A. Gunaydin, I. B.

Witten, K. Deisseroth, Dopamine neurons modulate neural encoding and expression of depression-related behaviour. *Nature* **493**, 537–541 (2013). doi:10.1038/nature11740 Medline

12. J.-L. Cao, H. E. Covington 3rd, A. K. Friedman, M. B. Wilkinson, J. J. Walsh, D. C. Cooper, E. J. Nestler, M. H. Han, Mesolimbic dopamine neurons in the brain reward circuit mediate susceptibility to social defeat and antidepressant action. *J. Neurosci.* **30**, 16453–16458 (2010). doi:10.1523/JNEUROSCI.3177-10.2010 Medline
13. S. A. Golden, H. E. Covington 3rd, O. Berton, S. J. Russo, A standardized protocol for repeated social defeat stress in mice. *Nat. Protoc.* **6**, 1183–1191 (2011). doi:10.1038/nprot.2011.361 Medline
14. M. J. Wanat, F. W. Hopf, G. D. Stuber, P. E. M. Phillips, A. Bonci, Corticotropin-releasing factor increases mouse ventral tegmental area dopamine neuron firing through a protein kinase C-dependent enhancement of Ih. *J. Physiol.* **586**, 2157–2170 (2008). doi:10.1113/jphysiol.2007.150078 Medline
15. H. Neuhoff, A. Neu, B. Liss, J. Roeper, I_h channels contribute to the different functional properties of identified dopaminergic subpopulations in the midbrain. *J. Neurosci.* **22**, 1290–1302 (2002). Medline
16. N. P. Poolos, M. Migliore, D. Johnston, Pharmacological upregulation of h-channels reduces the excitability of pyramidal neuron dendrites. *Nat. Neurosci.* **5**, 767–774 (2002). Medline
17. M. A. Frye, Bipolar disorder—a focus on depression. *N. Engl. J. Med.* **364**, 51–59 (2011). doi:10.1056/NEJMcp1000402 Medline
18. M. B. Wilkinson, C. Dias, J. Magida, M. Mazei-Robison, M. Lobo, P. Kennedy, D. Dietz, H. Covington 3rd, S. Russo, R. Neve, S. Ghose, C. Tamminga, E. J. Nestler, A novel role of the WNT-dishevelled-GSK3β signaling cascade in the mouse nucleus accumbens in a social defeat model of depression. *J. Neurosci.* **31**, 9084–9092 (2011). doi:10.1523/JNEUROSCI.0039-11.2011 Medline
19. Y. Nakatani, H. Masuko, T. Amano, The effect of lamotrigine on Na(v)1.4 voltage-gated sodium channels. *J. Pharmacol. Sci.* **123**, 203–206 (2013). doi:10.1254/jphs.13116SC Medline
20. M. Biel, C. Wahl-Schott, S. Michalakis, X. Zong, Hyperpolarization-activated cation channels: From genes to function. *Physiol. Rev.* **89**, 847–885 (2009). doi:10.1152/physrev.00029.2008 Medline
21. J. Zhang, M. S. Shapiro, Activity-dependent transcriptional regulation of M-Type (Kv7) K(+) channels by AKAP79/150-mediated NFAT actions. *Neuron* **76**, 1133–1146 (2012). doi:10.1016/j.neuron.2012.10.019 Medline
22. H. C. Tsai, F. Zhang, A. Adamantidis, G. D. Stuber, A. Bonci, L. de Lecea, K. Deisseroth, Phasic firing in dopaminergic neurons is sufficient for behavioral conditioning. *Science* **324**, 1080–1084 (2009). doi:10.1126/science.1168878 Medline
23. J. J. Walsh, A. K. Friedman, H. Sun, E. A. Heller, S. M. Ku, B. Juarez, V. L. Burnham, M. S. Mazei-Robison, D. Ferguson, S. A. Golden, J. W. Koo, D.

Chaudhury, D. J. Christoffel, L. Pomeranz, J. M. Friedman, S. J. Russo, E. J. Nestler, M. H. Han, Stress and CRF gate neural activation of BDNF in the mesolimbic reward pathway. *Nat. Neurosci.* **17**, 27–29 (2014). doi:10.1038/nn.3591 Medline

24. J. W. Koo, M. S. Mazei-Robison, D. Chaudhury, B. Juarez, Q. LaPlant, D. Ferguson, J. Feng, H. Sun, K. N. Scobie, D. Damez-Werno, M. Crumiller, Y. N. Ohnishi, Y. H. Ohnishi, E. Mouzon, D. M. Dietz, M. K. Lobo, R. L. Neve, S. J. Russo, M. H. Han, E. J. Nestler, BDNF is a negative modulator of morphine action. *Science* **338**, 124–128 (2012). doi:10.1126/science.1222265 Medline

25. E. B. Margolis, J. M. Mitchell, J. Ishikawa, G. O. Hjelmstad, H. L. Fields, Midbrain dopamine neurons: Projection target determines action potential duration and dopamine D(2) receptor inhibition. *J. Neurosci.* **28**, 8908–8913 (2008). doi:10.1523/JNEUROSCI.1526-08.2008 Medline

26. S. Lammel, A. Hetzel, O. Häckel, I. Jones, B. Liss, J. Roeper, Unique properties of mesoprefrontal neurons within a dual mesocorticolimbic dopamine system. *Neuron* **57**, 760–773 (2008). doi:10.1016/j.neuron.2008.01.022 Medline

27. G. Turrigiano, L. F. Abbott, E. Marder, Activity-dependent changes in the intrinsic properties of cultured neurons. *Science* **264**, 974–977 (1994). doi:10.1126/science.8178157 Medline

28. G. Turrigiano, Too many cooks? Intrinsic and synaptic homeostatic mechanisms in cortical circuit refinement. *Annu. Rev. Neurosci.* **34**, 89–103 (2011). doi:10.1146/annurev-neuro-060909-153238 Medline

29. A. Maffei, K. Nataraj, S. B. Nelson, G. G. Turrigiano, Potentiation of cortical inhibition by visual deprivation. *Nature* **443**, 81–84 (2006). doi:10.1038/nature05079 Medline

30. A. Destexhe, E. Marder, Plasticity in single neuron and circuit computations. *Nature* **431**, 789–795 (2004). doi:10.1038/nature03011 Medline

31. K. Whalley, Synaptic plasticity: Balancing firing rates in vivo. *Nat. Rev. Neurosci.* **14**, 820–821 (2013). doi:10.1038/nrn3637 Medline

32. D. K. Dickman, G. W. Davis, The schizophrenia susceptibility gene dysbindin controls synaptic homeostasis. *Science* **326**, 1127–1130 (2009). doi:10.1126/science.1179685 Medline

33. S. Lammel, B. K. Lim, C. Ran, K. W. Huang, M. J. Betley, K. M. Tye, K. Deisseroth, R. C. Malenka, Input-specific control of reward and aversion in the ventral tegmental area. *Nature* **491**, 212–217 (2012). doi:10.1038/nature11527 Medline

34. D. L. Wallace, M. H. Han, D. L. Graham, T. A. Green, V. Vialou, S. D. Iñiguez, J. L. Cao, A. Kirk, S. Chakravarty, A. Kumar, V. Krishnan, R. L. Neve, D. C. Cooper, C. A. Bolaños, M. Barrot, C. A. McClung, E. J. Nestler, CREB regulation of nucleus accumbens excitability mediates social isolation-induced behavioral deficits. *Nat. Neurosci.* **12**, 200–209 (2009). doi:10.1038/nn.2257 Medline